universität wien

MASTER'S THESIS

Title of the Master's Thesis

"Partial Wave Analysis as a tool for Central Exclusive Production Studies with ALICE"

submitted by

Deniz Mostarac BSc

in partial fulfilment of the requirements for the degree of

Master of Science (MSc)

Vienna, 2018

degree programme code as it appears on the student record sheet:	A 066 876
degree programme as it appears on the student record sheet:	Masterstudium Physik UG2002
Supervisor:	Hon.-Prof. Dipl.-Phys. Dr. Eberhard Widmann

Abstract

This master thesis was initially motivated by our desire to apply Partial Wave Analysis (PWA) to data from proton-proton collision in the central production regime with the ALICE detector of the LHC at CERN. This implied to work out and understand the formalism and then subsequently implement its phases and parts computationally. However, as with any project in its infancy, we did not have an idea of all the side-steps we would have to make to finally be able to be confident in analyzing such data and making appropriate conclusions from it. So what initially started as reworking a primer on PWA and reproducing results with our own programs, grew into a study of resonances, Regge theory, event simulation, statistics, hadron collisions, and reaction dynamics just to name a few. What is essentially going to follow is a work which will largely follow a primer-like structure, on selected topics, which altogether engulf, in my opinion, the necessary concepts and tools to perform such research as discussing Central Exclusive Production (CEP) in proton-proton collisions. The way in which I imagined this thesis is to first establish its nature, importance, and purpose by laying down the general framework which is, in this case, High Energy Particle diffraction. Afterward, I will introduce (or rather review) the necessary concepts in order to discuss Regge theory, and quite obviously so, introduce Regge theory itself, in its phenomenological form. Many of these concepts will be used through the thesis, whether as phenomenology or nomenclature. This will cover the background theory motivating the research and will allow me to delve into more technical parts of the work. This mainly consists of a part concerned with resonances, and a part on partial wave analysis. These parts will act mostly as isolated sections, containing the related theory, experimental approach (if applicable), and results (if applicable).

Table of Contents

1. Motivation and Outline

It might come as no surprise, that there are still "mysterious" parts of hadron physics phenomenology, not the least puzzling of which is hadronic diffraction, a subset of soft processes in hadronic collisions (Chapter 2). Our group, as a part of the ALICE collaboration at CERN, has access to a plethora of proton-proton collision data. A significant part of the contributing cross-sections is attributed to hadronic diffraction (20% of the total σ of $\approx$ 100mb). Within this sphere of interest, we choose to focus on recognizing and analyzing Central Exclusively Produced resonances (Chapter 4). Our motivation for doing so trickles down to the fact that the features of the ALICE detector (of which the significant ones for this research are the veto detectors $V0$, FMD, and (since run 2) AD, as together, they cover a pseudo-rapidity (η) range from -7 to $+$6.3.) allow for a precise selection of a signature, Double Gap Topology (rapidity) in exclusively centrally produced events (Chapter 3).

We made the assumption that the Central Exclusive Production cross-section is largely achieved by a Double Pomeron Exchange (DPE) mechanism. The theoretical foundation we used to justify our assumption for the dominant process is a phenomenological approach, namely, Regge theory (Chapters 3 and 4).
The main goal of this thesis was to, in addition to a standard invariant-mass analysis for identifying resonances in terms of mass, be able to recognize them in terms of their quantum numbers (partial waves). This proposes Partial Wave Analysis (PWA) as the natural approach since it allows us to interpret observed angular distributions of charged final states in the ALICE detector, in terms of sets of partial waves.

It is, however, important to note that Partial Wave Analysis as a tool is completely independent of the theory related to Central Exclusive Production and its phenomenology. Apart from having an assumption for the process one would analyze, in our case based on Regge theory, and including a model for the momentum dependence of the cross-section with a Monte-Carlo (MC) simulation (relevant for the efficiency corrections due to the detector properties), there is no conjunction between the two.
Regretfully, due to the time constraints, we haven't managed to apply partial wave analysis on to actual proton-proton ALICE data. This effectively means that the part of the thesis, which would merge the Regge theory-based model with the analysis tool which is PWA, is missing. So the reader can consider the parts dis-

cussing the theoretical foundation for hadronic diffraction and Central Exclusive Production (Chapters 2, 3, 4) as separate from the parts discussing PWA (Chapters 5, 6, 7).

Finally, because the disjointedness of the thesis, which basically threads through both theoretical and experimental water of particle physics, I find it useful to state that for clarifications of the discussion in Chapters related to Regge theory and hadron diffraction, one should refer to V. Barone and E. Predazzi [1] and Donnachie, S., Dosch, G., Landshoff, P., & Nachtmann, O. [2] (which I have made an extensive use of). For a more detailed and concise discussion on Partial Wave Analysis, on which our work has greatly been based upon, one should refer to Chung, S. U., Brose, J., Hackmann, R., Klempt, E., Spanier, S., & Strassburger, C. [3], Peters, K. [4] and Chung, S. U. [5].

2. Introduction to Diffractive Phenomena

In order to start talking about diffractive phenomena, we have to be a bit more explicit what we mean. The phenomenology that this term can cover is vast and diverse. Naturally, in this thesis, we deal with diffractive phenomena when seen as a subset of hadronic processes in particle physics. Hadronic processes are usually classified as either soft or hard, but for the purposes of this thesis, we will conveniently ignore hard processes except simply mentioning the key characteristics. It suffices to say that there is no unique energy scale for a hard process, except for being able to confidently say that large momentum exchanges ($\geq$ 1 GeV) are implied [1]. This means that we can use perturbative QCD to describe these reactions, at least partly. A typical, representative hard reaction would be large momentum transfer jet production.
Hadronic diffraction is typically in the soft regime. Soft processes really have only one characteristic scale, namely hadron size ($R \approx 1$ fm) [1]. Momentum interchange in the t-channel ($\propto (R^2)^{-1}$) is typically low, which implies suppression of large momentum interchange in the t-channel. This can easily be seen by observing that the t-dependent cross-section is exponential (e.g. $e^{-R^2|t|}$). The aforementioned presence of a large length scale makes perturbative QCD an inadequate theoretical description. A phenomenological description is found in the form of Regge theory, which is, to the best of my knowledge, still very much the de facto theory for soft hadronic processes.

What is exactly meant by hadronic diffraction is a bit tricky to discuss, since

one might expect a diffraction pattern whenever one hears the term diffraction. In the context of hadronic collisions, this is not necessarily related. However, it is reasonably simple to see how far the analogy goes and why this optical analogy is, in fact, a reasonable one.

Consider a light diffraction experiment, like in Born and Wolf [6], where S_0 is a monochromatic point source of angular frequency ω_0. The electric and magnetic fields are plane waves at a point P (Figure 1) in the image space, given by [7]:

$$E(P,t) = \Re(e(P)e^{-i\omega t}) \tag{2.1}$$
$$H(P,t) = \Im(h(P)e^{-i\omega t}) \tag{2.2}$$

The pupil (in analogy to the pupil of the eye) is considered as a diffraction aperture. Here, we infer that the short wavelength condition ($kR >> 1$, where k is the wave number and R is the pupil radius), and the Helmholtz equation are satisfied. The amplitudes for the waves immediately before the pupil are effectively mapped to some value at P in the image space, given by the Fresnel-Kirchhoff formula:

$$U(P) = -\frac{ik}{4\pi}U_0 \int^{pupilpoint} d^2\vec{b}(1+cos\chi)\frac{e^{iks}}{\vec{s}} \tag{2.3}$$

where $\vec{b}$ is a vector lying on the pupil plane, $\vec{s}$ the vector connecting P to the point made out by $\vec{b}$ and $cos\chi$ the inclination of $\vec{s}$ with respect to the normal to the pupil.

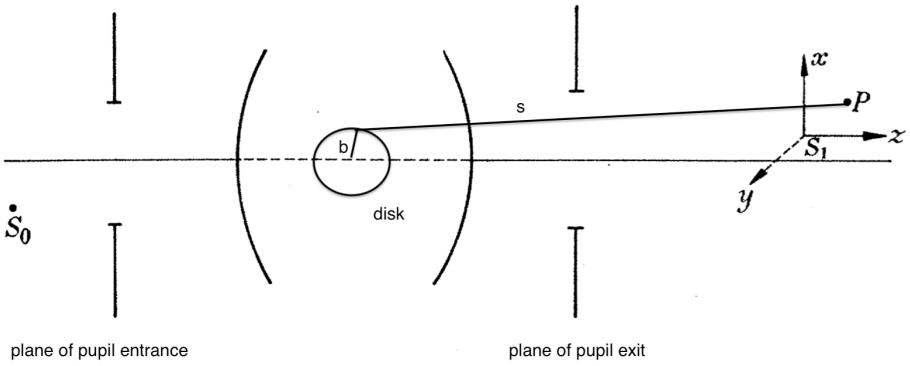

Figure 1 Schematical depiction of the pupil plane along with the monochromatic source.

The problem can be further simplified when considering $R/D << 1$ (where D denotes position of the light collection plane w.r.t the pupil exit plane), as we can consider Frauenhoffer diffraction ($kR^2/D << 1$, which is the region relevant for hadron physics purposes) and $\vec{s}$ as a power series expansion in $\vec{b}/\vec{r}$ (where $\vec{r} = \vec{b} + \vec{s}$). We can write the diffracted wave function at the point P in the Fraunhofer limit as:

$$U(P) = -\frac{ik}{2\pi} U_0 \frac{e^{ikr}}{r} \int_{disk} d^2b S(b) e^{-iqb} \tag{2.4}$$

where $q \approx k' - k$, given the assumptions, and given that we are talking about the small angle approximation (angle θ enclosed by r and the normal onto the pupil plane). $S(b)$ is given by $1 - \gamma(b)$, where $\gamma(b)$ is the profile function. We can see that (2.4) has the form of a spherical wave, multiplied by a factor which can be recognized to be the scattering amplitude. For azimuthally symmetric profile functions one can express the scattering cross-section as the Bessel transform of the profile function, which finally simplifies this discussion enough so we can make a clean analogy between hadronic diffraction and diffraction in optics.

Consider a profile function Γ, for a black disk, of the form (if in doubt that this is a viable analogy for a hadron physics scenario, I point out that Babirnet's principle as can be found in [7], ensures this):

$$\Gamma(b) = \begin{cases} 1 & b \leq R \\ 0 & b > R \end{cases} \tag{2.5}$$

The differential cross-section is given by the modulus squared of the amplitude, and has the following form (by the expansion of a Bessel function for small arguments, in this case, the angle θ) [1]:

$$\frac{d\sigma}{dcos\theta} = \frac{\pi k^2 R^4}{2} [1 - 1/4(kR\theta)^4] \tag{2.6}$$

With this, I finally establish what is meant by hadronic diffraction, as it can immediately be seen that cross-sections for soft processes as given above, expanded in to its power series around the low t-channel momentum interchange, have the same functional form ($|t|$ is proportional to θ^2 at high energies such as in the LHC) as the ones demonstrated for "ordinary" diffraction.

As far as defining diffraction purely in terms of hadronic physics, there is no unambiguous "definition". However, one can be explicit enough to highlight the appropriate phenomena. It necessarily has to be true that at high energies no quantum numbers have been exchanged between the colliding particles (or vacuum quantum numbers are exchanged). This definition is general enough to cover all cases (e.g single diffraction, double diffraction), but if not for the simple fact that it is experimentally rather difficult to establish if in fact vacuum numbers have been exchanged, one should rely on an additional phenomenological "definition", namely that a diffractive reaction is characterized by a large, non-exponentially suppressed, rapidity gap in the final state (discussion in Chapter 4 Section 3) [1].

However, if we really want to be explicit, we should rely on a definition based on the theory describing the process. "Regge theory describes hadronic reactions at high energies in terms of the exchange of 'objects' called Reggeons. The Reggeon with vacuum quantum numbers, which dominates asymptotically, is the so-called Pomeron" [1].

3. Properties of the S-Matrix

Before I arrive at Regge theory itself, I will need to, for the sake of completeness, touch on some principle concepts and nomenclature.

For a complete set of orthonormal states i (initial) and f (final), the probability that a state i has become the state f after a scattering is given by [8]:

$$P_{fi} = |\langle f|S|i\rangle|^2 = \langle i|S^\dagger|f\rangle \langle f|S|i\rangle \tag{3.1}$$

where $\langle f|S|i\rangle$ is the S-Matrix element. The S-Matrix is necessarily required to be a linear operator by the superposition principle, to be constructed from Lorentz invariant quantities, as well as possessing the properties of unitarity, analyticity and crossing symmetry. The S-Matrix is related to the transition matrix T in the following way:

$$\langle f|S|i\rangle = \delta_{fi} + iT_{if} \tag{3.2}$$

where the T-Matrix can be rewritten as to give the following:

$$\langle f|S|i\rangle = \delta_{fi} + I(2\pi)^4\delta^4(P^f - P^i)A(i \to f) \tag{3.3}$$

where I denotes the identity operator, $A(i \to f)$ is the transition amplitude, while P^f and P^i denote the momenta in the final and the initial state. In this way, we

have introduced the familiar relativistic scattering amplitude, as in the definition of the differential cross-section, given by:

$$d\sigma = \frac{1}{\Phi}|A(i \to f_n)|^2 d\Pi_n \tag{3.4}$$

where Φ is the incident flux and Π is the Lorentz invariant phase space factor (with an implicit sum over all of the final n states) [21].

A convenient and recurrent formation of the relativistic scattering amplitude throughout this thesis is in terms of partial waves. One can express the Mandelstam variables (s, u, t) in terms of the CM frame variables to arrive at formidably complex expressions. However, these simplify greatly in high energy particle physics since at LHC energies hadron masses are small enough to be considered as being equal one to another. We can use the following relation to rewrite amplitudes in terms of e.g s and $\cos(\theta)$:

$$\cos(\theta) = 1 + \frac{2t}{s - 4m^2} \tag{3.5}$$

to finally arrive at the following form of the relativistic scattering amplitude:

$$A(s, cos\theta) = \sum_{l=0}^{\infty}(2l+1)A_l(s)P_l(cos\theta) \tag{3.6}$$

where l stands for the angular momentum quantum number, $P_l(cos\theta)$ denotes the Legendre polynomials, and the partial wave amplitudes are given by [2]:

$$A_l(s) = \frac{1}{2}\int_{-1}^{1} dcos\theta P_l(cos\theta)A(s, cos\theta) \tag{3.7}$$

Within the framework of non-relativistic quantum mechanics, bound states fall into families with increasing energy and angular momentum. These bound states appear as poles of the S-matrix, or equivalently as poles of the partial wave amplitudes. Regge theory essentially takes this, while allowing for complex angular momenta. One insinuates the existence of an interpolating function which reduces to the partial wave amplitudes for real-valued angular momenta. One can assume that it is possible that these singularities turn out to be simple "moving" poles (Regge poles) [2]. Clearly, the existence of such poles in terms of the S-Matrix is a conjecture, which turns out to be true nonetheless.

So, in essence, we claim that the properties of the S-Matrix allow for the relativistic partial wave amplitude to be uniquely and analytically continued to complex angular momenta [2].

3.1 Unitarity of the S-Matrix

The completeness and orthonormality of the states used in defining the S-Matrix element in formula (3.1) implies that the sum of the moduli squared over all states must amount to unity. This can also be trivially seen from probability theory. This restricts possible S-Matrices to unitary ones. The unitarity condition can be written in terms of the transition matrix as:

$$\langle j|T|i\rangle - \langle j|T^\dagger|i\rangle = (2\pi)^4 i \sum_f \delta^4(P^f - P^i) \langle j|T^\dagger|f\rangle \langle f|T|i\rangle \tag{3.8}$$

from where in terms of the amplitudes, it directly follows that:

$$2\Im(A(i \to f)) = \sum_n \int d\Pi_n A^*(f \to n) A(i \to n) \tag{3.9}$$

where Π_n denotes an integration over all momenta, summed over all discrete quantum numbers.
In the special case where we consider the i and f states to be identical, e.g forward elastic scattering ($t = 0$), the right-hand side is proportional to the total cross-section. This expression tells us that the total cross-section, for any reaction, can be calculated from only the matrix element for elastic scattering in the forward direction (the optical theorem) [8].

It is instructive to note that, as the energy increases, the total cross-section, given by:

$$\sigma_{tot} = \frac{2}{\Phi} \Im(A_{el}(s, t = 0)) \tag{3.10}$$

which is a summation over an increasing number of possible channels, certainly remains nonzero. $A_{el}(s, t = 0)$ is the amplitude for elastic scattering in the forward direction, while Φ is the flux factor (for a 2 particle transition, the flux factor would be the probability for each of the particles to be found in unit phase space volume respectively, multiplied by their relative velocity).
Hence, the imaginary part of the amplitude has to be nonzero implicitly, which doesn't necessarily have to be true for the real part of the amplitude [1]. At this point, we note that hadronic diffraction exhibits the same "leading particle effect" as do elastic collisions, which comes from the optical theorem [1].

3.2 Analyticity of the S-Matrix

There is an obvious truth, most simply noticed, order by order, from Feynman diagrams, which is the basic principle of crossing symmetry. This comes from the fact that the same functional form of the scattering amplitude (consider it as $f(u,s,t)$), analytically continued to physical kinematic regions (s, t, u as complex variables), can represent a reaction in different, nonoverlapping kinematic regions. We implicitly assume that such analyticity is possible and that taking only the real part reproduces physical amplitudes.

Consider a generic scattering s-channel process $a+b \to c+d$. We can certainly write an amplitude, dependent on the Mandelstam variables. Assuming that all masses are equal, the physical kinematic region is defined as $s >$max$[(m_a + m_b),(m_c+m_d)]$ and $(u,t)<0$. The amplitude can, by our assumption, be analytically continued to cover $t >$max$[(m_a+m_c),(m_b+m_d)]$ and $(s,u)<0$, for a t-channel process $a+c \to b+d$ (likewise for a u-channel process).

Consider the complex s-channel for the aforementioned process (Figure 2). There is a cut from $4m^2$ to ∞, due to physical thresholds in the s-channel. The simple pole at $4m^2$ is interpreted as a bound state of mass $m=\sqrt{s}$. There are further branch points and their respective cuts present. If we consider s and t to be the independent variables, there are singularities and cuts present, due to the physical thresholds in the u-channel, namely a cut at $s = 4m^2 - t - u_0$, where u_0 is the singularity in the u-channel [2]. As before, additional cuts occur, due to branch points in both channels (t is implicitly held fixed).

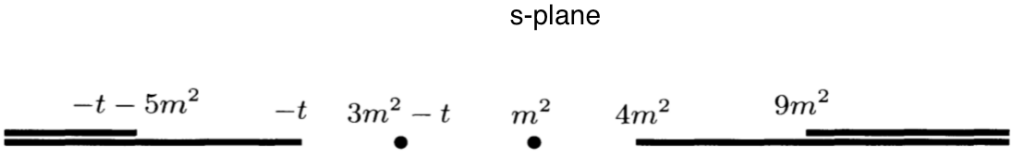

Figure 2 Singularities (dots) and cuts (lines) of the scattering amplitude in the complex s-plane. Figure is taken from V. Barone and E. Predazzi [1].

We should underlay the standard way in which we can "reach", as a representative example, in this case, the physical s-channel amplitude.
One defines the discontinuity over the cut due to the physical thresholds in the s-channel as:

$$D_s(s,t,u) = A(s+i\epsilon,t) - A(s-i\epsilon,t) \tag{3.11}$$

where, since the amplitude exclusively takes well defined values on the real axis of the complex s-space ($-t < s < 4m^2$), by Schwarz reflection principle, this corresponds to the imaginary part of the amplitude ($D_s(s,t,u) = 2i\Im(A(s + i\epsilon, t))$) [2]. By crossing symmetry we have:

$$D_t(s,t,u) = A(s,t+i\epsilon) - A(s,t-i\epsilon) = 2i\Im(A(s,t+i\epsilon)) \qquad (3.12)$$
$$t > 4m^2 \quad and \quad u,s \leq 0$$
$$D_u(s,t,u) = A(s,u+i\epsilon) - A(s,u-i\epsilon) = 2i\Im(A(s,u+i\epsilon)) \qquad (3.13)$$
$$u > 4m^2 \quad and \quad s,t \leq 0$$

An amplitude with well defined analytic properties allows for a dispersion relation, which is used, in this context, as an integral representation of complex functions. These are used to determine complex functions, just from the knowledge of the real or imaginary part. Let's take the Cauchy integral representation of the amplitude. We take a closed, positively oriented curve, as in Figure 3, where one can neglect the half circles based on the assumption that the amplitude goes to 0 as we take the radius to infinity. The amplitude is given by:

$$A(s,t) = \frac{g_s^2}{s-s_B} + \frac{g_u^2}{u-u_B} + \frac{1}{2\pi i}\int_{s_0}^{\infty} ds^{'} \frac{D_s(s^{'},t,u^{'})}{s^{'}-s} + \frac{1}{2\pi i}\int_{u_0}^{\infty} du^{'} \frac{D_u(s^{'},t,u^{'})}{u^{'}-u} \qquad (3.14)$$

where the first two terms are the pole contributions (s_B and u_B denote the bound-state pole position in the respective channel), and g_s and g_u are the residues. The integral limits are due to the lowest state thresholds for a given channel.
One can manipulate the definition of the discontinuities across the cut to include any bound state, e.g. for $s < 4m^2$ we say that:

$$D_s(s,t,u) = -2\pi i g_s^2 \delta(s - s_B) \qquad (3.15)$$

which allows for a much cleaner expression of Eq. (3.14). Across the discontinuity, one approaches the real axis from above (akin to the $i\epsilon$ prescription). This prescription is added to the denominator to ensure it doesn't vanish.

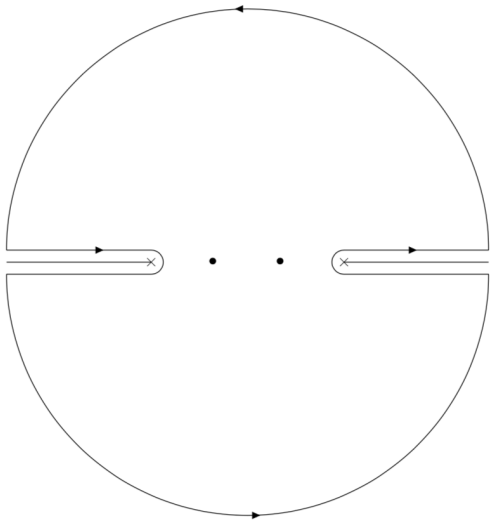

Figure 3 The contour of integration in the complex s-plane. Singularities are denoted by dotes, cuts by lines, and branch points by crosses. Figure taken from Donnachie, S., Dosch, G., Landshoff, P., & Nachtmann, O. [2].

Remember that for any function that is analytic on the whole real line except at a point (e.g simple pole), the Cauchy principal value is defined to as (provided that all the limits exist) [9]:

$$p.v(\int_{-\infty}^{\infty} f(x)dx) \coloneqq \lim_{r\to 0^+}[\int_a^{c-r} f(x)dx + \int_{c+r}^{b} f(x)dx] \tag{3.16}$$

The 2 segments are joined by a half-circle S_r, for which it is assumed that it is small enough that $f(x)$ remains in its region of analyticity. For a circular arc around the pole, defined by:

$$T_r : \quad z = c + re^{i\theta} \quad (\theta_1 \leq \theta \leq \theta_2) \tag{3.17}$$

the integral amounts to:

$$\lim_{r\to 0^+} \int_{T_r} f(z)dz = i(\theta_2 - \theta_1)Res(f;c) \tag{3.18}$$

where $Res(f;c)$ is the residue of f at c, which for a half-circle amounts to:

$$\lim_{r\to 0^+} \int_{half-circle} f(z)dz = i\pi Res(f;c) \tag{3.19}$$

This allows us to write a Cauchy integral as given above, in the following form:

$$\oint_{\Gamma'_\epsilon} \frac{f(\zeta)}{\zeta - z_0}d\zeta = p.v \int_\Gamma \frac{f(\zeta)}{\zeta - z_0}d\zeta + i\pi f(z_0) \tag{3.20}$$

This is a more general version of the standard "trick" in particle physics, for functions akin to the denominators in Eq. (3.14). It is, therefore, equivalent to write the formula (3.14) as [2]:

$$\Re(A(s,t)) = \frac{1}{2\pi i} p.v \int_0^\infty ds^{'} \frac{D_s(s^{'},t,u^{'})}{s^{'}-s} + \frac{1}{2\pi i} p.v \int_0^\infty du^{'} \frac{D_u(s^{'},t,u^{'})}{u^{'}-u} \quad (3.21)$$

Let $f(x)$ be a function that is described by a dispersion relation, as is the one given above. Let $g(x)$ be a function that is described by a dispersion relation, and has a specified value $g(x_1)$ at x_1. The dispersion relation for $g(x)$ with such a constraint can be obtained easily if one defines [10]:

$$f(x) \equiv \frac{g(x) - g(x_1)}{x - x_1} \quad (3.22)$$

Note that $f(x)$ is clearly analytic at x_1. From the definition, it follows that it is equal to the gradient of $g(x)$ at that point, which we consider to be well defined. If $f(x)$ has a branch point at x_0, than $g(x)$ has to also have one at that point. Putting this in the Cauchy integral representation for f gives:

$$\frac{g(z)-g(x_1)}{z-x_1} = \frac{1}{2\pi i}\left[\int_{x_0}^\infty \frac{g(x^{'}+i\epsilon)-g(x_1)}{(x^{'}-x_1)(x^{'}-z)}dx^{'} - \int_{x_0}^\infty \frac{g(x^{'}-i\epsilon)-g(x_1)}{(x^{'}-x_1)(x^{'}-z)}dx^{'}\right] =>$$
$$g(z) = g(x_1) + \frac{z-x_1}{2\pi i}\int_{x_0}^\infty \frac{g(x^{'}+i\epsilon)-g(g(x^{'}-i\epsilon)}{(x^{'}-x_1)(x^{'}-z)}dx^{'} \quad (3.23)$$

This is called the subtracted dispersion relation [15]. This is an essential technique if the amplitude, in fact, doesn't tend to 0 sufficiently quickly to neglect the integral over the half circle. But $A/(s^{'}-s)$ might do so. In fact, for cases in Regge theory where the total cross-section becomes constant asymptotically, two subtractions are necessary to obtain the amplitude for forward elastic scattering [1].
There are several ways to go about the aforementioned function $g(x)$. Discussion of this in greater detail serves no purpose for this thesis, but I will present a standard way in which N-times dispersion relations are given, in the case where the amplitude behaves asymptotically:

$$A(s,t) \propto s^\lambda \quad \text{as} \quad s \to \infty \quad (3.24)$$

namely [1]:

$$A(s,t) = \sum_{n=0}^{N-1} c_n(t)s^n + \frac{1}{\pi}(s-s_1)...(s-s_N)\int_{4m^2}^{\infty} \frac{D_s(s^{'},t)}{(s-s_1)...(s^{'}-s_N)(s^{'}-s)}ds^{'} + \frac{1}{\pi}(u-u_1)...(u-u_N)\int_{4m^2}^{\infty} \frac{D_u(u^{'},t)}{(u-u_1)...(u^{'}-u_N)(u^{'}-u)}du^{'} \tag{3.25}$$

where N is the smallest integer greater than λ. Here u_i is given by:

$$u_i = 4m^2 - s_i - t \tag{3.26}$$

This clarifies the statement that one needs two subtractions to the amplitude for the forward elastic scattering. In this formulation, we need only the total cross-section and 2 unknown coefficients (we can fit for these, but are in general arbitrary from the calculation), to completely determine the dispersion relation.

3.3 The Froissart-Gribov Representation

As this thesis will largely make use of the partial wave basis, amplitudes for which we have a dispersion relation, or more precisely their partial wave amplitudes, will be expressed in the Froissart-Gribov representation.

As an extension to the amplitudes, as described in the section above (remember the asymptotic behavior as $s \to \infty$ given in (3.24)), we re-express the amplitude in terms of the scattering angle z_t, by the following relation:

$$z_t \equiv cos\theta_t = 1 + \frac{2s}{t-4m^2} = 1 + \frac{2s}{t-4m^2} = -(1 + \frac{2u}{t-4m^2}) \tag{3.27}$$

The N-times subtracted relation for a fixed t, at $z_t = 0$, is than given by:

$$A(z_t,t) = \sum_{n=0}^{N-1} c_n(t)z_t^n + \frac{z_t^N}{\pi}\int_{z_0}^{\infty} \frac{D_s(s^{'}(z_t^{'},t),t)}{z_t^{'N}(z_t^{'}-z_t)dz_t^{'}} + \frac{z_t^N}{\pi}\int_{-z_0}^{\infty} \frac{D_u(u^{'}(z_t^{'},t),t)}{z_t^{'N}(z_t^{'}-z_t)dz_t^{'}} \tag{3.28}$$

where N is the smallest integer larger than λ, as in (3.24). We can substitute this in the expression for the partial wave amplitudes (3.7), where we recognize the functional form of the Legendre functions of the second kind:

$$Q_l(z_t^{'}) = \frac{1}{2}\int_{-1}^{1} dz_t P_l(z_t) \frac{z_t^N}{z_t^{N'}(z_t^{'} - z_t)} \quad l \geq N$$

This finally gives a clean expression for the partial wave amplitude (Froissart-Gribov representation) [1]:

$$\begin{aligned} A_l(t) = &\frac{1}{\pi}\int_{z_0}^{\infty} dz_t D_s(s(z_t,t),t) Q_l(z_t) \\ &+\frac{1}{\pi}\int_{-z_0}^{-\infty} dz_t D_u(u(z_t,t),t) Q_l(z_t) \end{aligned} \tag{3.29}$$

4. Regge Theory

4.1 Virtual particles in t-channel models, and convergence.

The t-channel models, to which Regge theory belongs, describe reactions in terms of an interchange of "something" in the t-channel. We discuss this in terms of virtual particle exchanges (think virtual photons, in electromagnetic interactions). In any case, this picture fails for high energies [1].

As established with Eq. (3.6), the scattering amplitude for an exchange of a particle (e.g meson) with spin (J) and mass (M), is proportional to [2]:

$$A_{particle}(s,t) \propto A_J(t) P_J(cos\theta_t) \tag{4.1}$$

We introduced the notion that an exchange of a single particle comes from a pole singularity in the amplitude. Hence, we can establish jet another proportionality, namely:

$$A_{particle}(s,t) \propto \frac{P_J(cos\theta_t)}{t - M^2} \tag{4.2}$$

In a, at this point well-established fashion, we fix t and let $s \to \infty$. As $P_l(z_t) \propto z^l$, $A_{particle} \propto s^J$. From the unitary condition and the optical theorem one can conclude that [1]:

$$\sigma_{tot} = \frac{1}{s}\Im(A)(s, t=0) \underset{s\to\infty}{\sim} s^{2J-2} \tag{4.3}$$

This violates unitarity. In 4-dimensional spacetimes, there is a maximal rate of increase of the total cross-section, which still conserves unitarity. This is called the Froissart-Martin bound, and it is exactly what is violated by Eq. (4.2), for $J > 1$.

We continue with some further remarks on the convergence of partial waves, where we once again give the scattering amplitude in the s-channel :

$$A(s,z) = \sum_{l=0}^{\infty} (2l+1) A_l(s) P_l(z) \tag{4.4}$$

$$A_l(s) = \frac{1}{2}\int_{-1}^{1} dz P_l(z) A(s, t(z,s)) \tag{4.5}$$

$$z \equiv \cos(\theta) = 1 + \frac{2t}{s - 4m^2} \tag{4.6}$$

We can establish a notion of where the scattering amplitude is certainly well defined, but it is not clear if it also converges on a region large enough to contain at least a part of, in this case, t and u regions. If we acknowledge the asymptotic behavior of the Legendre polynomials, $P_l(cos\theta)$, for real angular momenta, given by:

$$P_l(cos\theta) = \mathcal{O}(e^{l|\Im(\theta)|}) \tag{4.7}$$

the partial wave amplitude must go as:

$$A_l(s) \propto e^{l\eta(s)} \tag{4.8}$$

$$|\Im(\theta)| \leq \eta(s) \tag{4.9}$$

for $l \to \infty$. This means that for any finite s, a partial wave base as stated above, cannot be extended so that it is defined on a region where t or u can become arbitrarily large [1].

4.2 Regge trajectories

The following section will be very limited and will not fully deal with the set of assumptions we will make. It is here to demonstrate a simple Regge trajectory and the underlying framework, as our work was focused on understanding and testing, rather than questioning the properties and details. However, a discussion in some depth is, in my opinion, necessary in order to begin doing related work, so I will present it here.

The crucial, base assumption is that one can extend partial wave amplitudes to complex values of angular momenta. We introduce an interpolation function $A(l, s)$, which by assumption corresponds to the partial wave amplitudes for real integer values of l. We also claim that the interpolating function has exclusively isolated singularities in the complex l plane, and is certainly holomorphic for some l such that $\Re(l) \geq L$. This means that there is a countable, finite number of singularities of the interpolating function in the complex l plane. Finally, we require that the interpolating function converges to 0 as the angular momenta go to infinity in magnitude, where the real part of l remains a positive integer.

A partial wave expansion in terms of the perceived interpolating function can

be written as:

$$A(s,z) = \sum_{l=0}^{N-1}(2l-1)A_l(s)P_l(z) - \frac{1}{2i}\int_C (2l-1)A(l,s)\frac{P_l(-z)}{\sin(\pi l)}dl \tag{4.10}$$

The integrand in the expression has residues for all $n > N$, which is the first value greater than L from the set of assumptions made in this chapter, given by (note that $P_n(-z) = (-1)^n P_n(z)$):

$$Res[f(l)]|_{j=n} = 2i(2n+1)A_n(s)P_n(z) \tag{4.11}$$

Consider a contour, as given in Figures 4 and 5. One can easily imagine what is in fact transpiring, by a simple deformation. Instead as in the picture, one can align the contour along the imaginary axis, without changing the value of the integral along it.

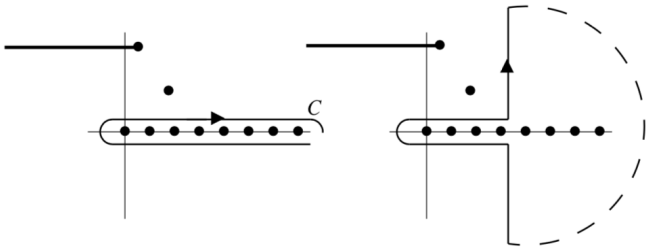

Figure 4 The contour of integration in the complex l-plane surrounding the poles at integer l. Notice the pole of $A(s,z)$ and the branch point with its cut. Figure taken from Donnachie, S., Dosch, G., Landshoff, P., & Nachtmann, O. [2].

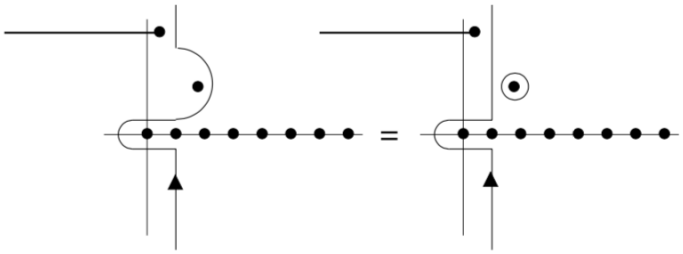

Figure 5 The result of moving the contour past the pole of $A(s,z)$. Figure taken from Donnachie, S., Dosch, G., Landshoff, P., & Nachtmann, O. [2].

As the contour moves toward lower values of $\Re(l)$, we get contributions from simple poles of the interpolation $A(s,z)$ and singularities from the $\sin(\pi l)$, which cancel some of the terms in the sum, leaving us with the following expression (Watson-Sommerfeld representation) [2]:

$$A(s,z) = -\sum_i \pi(2\alpha_i(s)+1)\beta_i(s)\frac{P_{\alpha_i}(-z)}{\sin(\pi\alpha_i)} - \frac{1}{2i}\int_{c-i\infty}^{c+i\infty}(2l+1)A(l,s)\frac{P_l(-z)}{\sin(\pi l)}dl \tag{4.12}$$

where α_i is the position of the pole, β is its residue and c is some position on the real axis of the complex plane to which we move the contour.
Consider that, since the Legendre polynomials behave as $P_l(z) \sim z^l$, for values of l greater than c, for large t and fixed s [11], the integral doesn't contribute asymptotically, and we are left with:

$$A(s,t) \simeq -\sum_i \beta_i(s)\frac{-z^{\alpha_i(s)}}{\sin(\pi\alpha_i(s))} \tag{4.13}$$

The dominant term is called the Regge trajectory, where the following proportionality holds [1]:

$$A(s,t) \sim -\beta(s)\frac{t^{\alpha(s)}}{\sin(\pi\alpha(s))} \quad \text{as} \quad t\to\infty \tag{4.14}$$

Completely analog calculations can be done in any other channel. The conclusion from Eq. (4.14), in words, is that the dominant contribution to the amplitude in the asymptotic t region is the leading singularly in the crossed s-channel.

This conclusion is more complicated in the presence of cuts, as is usually the case. Most importantly, there will be an added term to Eq. (4.14), namely:

$$-\frac{1}{2i}\int_\Gamma (2l+1)D_\Gamma A(l,s)\frac{P_l(-z)}{\sin(\pi l)}dl \tag{4.15}$$

where Γ is the contour from the branch point, along the cut. By $D_\Gamma A(l,s)$ we denote the discontinuity of the $A(l,s)$ across the cut. As we established above, in the presence of a Regge pole, the partial wave amplitude $A(l,t)$ behaves for $l\to\alpha(t)$ as [2]:

$$A(l,t) \approx \frac{\beta(t)}{l-\alpha(t)} \tag{4.16}$$

As a matter of fact, in his original proposition, Regge was concerned with potentials that can be represented as a superposition of screened Coulomb potentials (Yukawa potential), given in the following form:

$$V(r) = -V_0 \frac{e^{-\alpha r}}{r} \tag{4.17}$$

where α is the fine-structure constant, and Z is the atomic number. In this case, the singularities of the complex interpolating amplitude are poles for which the relation $\alpha(t) = l$ holds. Regge poles correspond to particles or bound states, and obtain integer l values, at some nonphysical value of t. We can take t to be close to t_0, where we chose t_0 such that $\Re(t0) = \sigma$ [12]. We can expand around $t = t_0$, resulting in:

$$\Re(\alpha(t)) = \sigma + \alpha^{'}(t - t_0) + ... \tag{4.18}$$

The amplitude obtains the following form [2]:

$$A_\sigma(t) \approx -\frac{\beta(t_0)/\alpha^{'}}{t - t_0 + i\Im(\alpha(t_0))/\alpha^{'}} \tag{4.19}$$

which we recognize as a Breit-Wigner for a resonance with a width given by:

$$\Gamma = \frac{\Im(\alpha(m_R^2))}{\alpha^{'} m_R} \tag{4.20}$$

and a mass m_R, such that $m_R^2 = t_0$. We will discuss resonances in depth later in the thesis.
We can see from (4.19) that Regge poles represent resonances and bound states of angular momentum, where what we call the trajectory, effectively interpolates these bound states. One usually parametrizes the trajectories as a linear function of t. This allows distinguishing trajectories in terms of intercept and slope.

We know as a matter of experimental fact, that hadronic total cross-sections are rising at very high energies, except for a basically flat region around $\sqrt{s} \propto (10-20)$ GeV^2. This flat region can only be compensated by a Regge trajectory with an intercept of 1, as introduced by Gribov, V. N. [13], named the Pomeron. This trajectory doesn't have a known, corresponding particle, and its recurrences are expected to be glueballs.

The Pomeron is the dominant contributor to the amplitudes for diffractive processes as well as elastic processes, which are also characterized by no quantum

numbers being exchanged between the constituents [1]. It has the following quantum numbers:

$$\textcircled{P}: \qquad P=+1 \qquad C=+1 \qquad G=+1 \qquad I=0 \qquad \xi=+1$$

where ξ is the signature quantum number. There is an addendum we must make, in order to present the relevant results for this thesis. We regard this as a technicality, which I find adequate here. Note that it is a much more involved and fundamental discussion than presented. We write the Froissart-Gribov representation, introduced in (3.29), in a slightly different form. We make a change of variables and use the properties of the Legendre functions of the second kind:

$$Q_l(-z_t) = -e^{i\pi l} Q_l(z_t) \tag{4.21}$$

With this, we arrive at a more symmetric expression, given by:

$$A_l(t) = \frac{1}{\pi}\int_{z_0}^{\infty} [D_s(s(z_t,t),t) + e^{-i\pi l} D_n(s(z_t,t),t)] Q_l(z_t) dz \tag{4.22}$$

We take the limit $l \to \infty$, where Q_l's asymptotically approximate to the following form [11]:

$$Q_l(z) \sim l^{-1/2} \exp[-(l+\frac{1}{2})\zeta(z)] \tag{4.23}$$

where $\zeta(z)$ is given by:

$$\zeta(z) = \ln[z + (z^2-1)^{1/2}] \tag{4.24}$$

The exponential goes to ∞ as we approach large values of $\Im(l)$. One can amend this issue by extrapolating the signature quantum number and a slight redefinition of the amplitude. We distinguish between even l amplitudes (A_l^+) and odd l amplitudes (A_l^-), and express this through the signature number as:

$$A_l^{\xi}(t) = \frac{1}{\pi}\int_{z_0}^{\infty} D_s^{\xi}(s,t) Q_l(z_t) dz_t \tag{4.25}$$

where the signatured discontinuity is given by:

$$D_s^{\xi}(s,t) \equiv D_s(s,t) + \xi D_u(s,t) \tag{4.26}$$

and A_l^{ξ} is related to the signatured partial wave amplitude by:

$$A_l(t) = \frac{1}{2}\sum_{\pm 1} (1 - \xi e^{-i\pi l}) A_l^{\xi}(t) \tag{4.27}$$

The Watson-Sommerfeld representation of the partial wave expansion for the signatured amplitude looks like [1]:

$$A(z_t,t)^{\xi} = -\sum_{i\xi}\pi(2\alpha_{i\xi}(s)+1)\beta_{i\xi}\frac{P_{\alpha_{i\xi}}(-z)}{\sin(\pi\alpha_{i\xi})} - \frac{1}{2i}\int_{c-i\infty}^{c+i\infty}(2l+1)A(l,s)\frac{P_l(-z)}{\sin(\pi l)}dl \tag{4.28}$$

where we sum over definite-signature Regge poles. Once again, we take the asymptotic approach, where the sum dominates the integral, and we recognize the leading pole behavior. We use the relation $P_l(z) \sim z^l$ to arrive at the following expression:

$$A(s,t) \sim -\beta(s)\frac{1-\xi e^{-i\pi\alpha(t)}}{\sin(\pi\alpha(t))}s^{\alpha(t)} \tag{4.29}$$

Previous conclusions made in this section remain unchanged. This expression has the added benefit that it actually does respect the assumptions we initially made. Let's give a simple amplitude for a Pomeron dominated process, such as the forward elastic scattering amplitude [1]:

$$A_{\textcircled{P}}(s,t=0) \simeq i\beta_{\textcircled{P}}(0)s^{\alpha_{\textcircled{P}}(0)} \tag{4.30}$$

where we used the limit:

$$\lim_{x\to 1}\frac{1+e^{-i\pi x}}{\sin(\pi x)} = -i \tag{4.31}$$

4.3 Diffractive Dissociation and Central Exclusive Production

Before getting into the detailed structure of diffractive processes, I must state the results we will use throughout this chapter. However, I will just state these as facts, without trying to convince the reader that they are true (a complete discussion can be found in Donnachie, S., Dosch, G., Landshoff, P., & Nachtmann, O. [2]). Firstly, we will make extensive use of the factorization of Regge theory when a single Regge trajectory dominates the process, and in absence of Regge cuts. The residue of a Regge pole factorizes to couplings at each vertex of a Reggeon Exchange Diagram.

Furthermore, we will make use of the generalized optical theorem (Muller's optical theorem), which relates tree body forward elastic amplitudes to inclusive cross-sections, and is given by [1]:

$$(2\pi)^3 2E\frac{d^3\sigma}{d^3p} = \frac{1}{s}Disc_{M^2}A_{12\bar{3}}(s,t,M^2) \tag{4.32}$$

where the discontinuity at $M^2 = (p_1 + p_2 - p_3)^2$ is given by:

$$Disc_{M^2}A_{12\bar{3}}(s,t,M^2) = \frac{1}{2i}[A_{12\bar{3}}(s,t,M^2+i\epsilon) - A_{12\bar{3}}(s,t,M^2-i\epsilon)] \tag{4.33}$$

A visual mnemonic of this manipulation is shown in Figure 6.

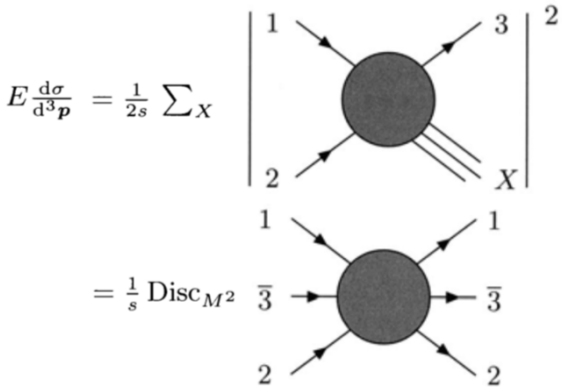

Figure 6 Visual representation of Muller's optical theorem. Note that this also sets up the initial reaction configuration (not necessarily unique). Figure is taken form V. Barone and E. Predazzi [1].

Let's tackle single diffractive dissociation, as it is the simplest case and gives all the necessary pieces to make Central Exclusive Production explicit. We will naturally make some reasonable approximations, as they will simplify the matter significantly. Consider the reaction $1+2 \to 3+X$. In the center of mass frame we can use customary relations, which in the asymptotic case, where we assume that the masses of X, M, and s are significantly greater than the remaining particle masses, give the following relations:

$$|p| = p_z \simeq \frac{\sqrt{s}}{2} \qquad E_1, E_2 \simeq \frac{\sqrt{s}}{2} \tag{4.34}$$

$$|p^{'}| \simeq |p_z^{'}| \simeq \frac{s-M^2}{2\sqrt{s}} \qquad E_3 \simeq \frac{s-M^2}{2\sqrt{s}} \tag{4.35}$$

where, after the collision, we used the fact that, transverse momenta of the outgoing particles are very small (outgoing momenta are denoted by a prime). Hence, we neglect that component completely. Diffraction requires low momentum interchange in the t-channel. We, therefore, require that the ratio of the magnitude for the momentum of particle 3 and the momentum of particle 1 is close to 1. This is precisely the definition of the Feynman variable x_f. The value of the ratio which we require corresponds to the so-called fragmentation region.

In terms of rapidity, one can easily obtain the following expression (in our limit for particle 3), namely:

$$y_3 = \frac{1}{2}\ln\frac{E_3 + p_z^{'}}{E_3 - p_z^{'}} \simeq \ln\frac{\sqrt{s}}{m_t} \tag{4.36}$$

where m_t is defined as:

$$m_t = \sqrt{m^2 + p_t^2} \quad \text{where} \quad p_t = (p_x, p_y, 0) \tag{4.37}$$

Particle X exhibits a range of possible rapidities, for which it should be clear that the lower bound is obtained if the particle is much heavier than the rest of the particles (which we take to be of same mass. At the energy scale of the LHC, this should make no difference) and obtains a fraction of the momentum proportional to the ratio of mass of the rest of the particles (one of them) and its mass M. Therefore, the biggest gap in rapidity between particle 3 and X should be given by:

$$\Delta y \simeq \ln\frac{\sqrt{s}}{m} + \ln\frac{m\sqrt{s}}{M^2} \simeq \ln\frac{s}{M^2} \tag{4.38}$$

The requirement which restricts us to the fragmentation region means that $M^2/s \approx 0$. Hence, the rapidity gap must be comparatively large. This is, in fact, the consideration which goes into the argument for the Double Gap Topology for Central Exclusive Production.

We refine our prior limit by taking $s >> M^2 >> t$, which doesn't change anything in the calculations above. The scattering amplitude is given by [1]:

$$A(12 \to 3X) \underset{s\to\infty}{\sim} \sum_i g_{13}^i(t) g_{2X}^i(t) \eta_i(t) (\frac{s}{M^2})^{\alpha_i(t)} \tag{4.39}$$

where $\eta_i(t)$ are the signature factors, given by:

$$\eta_i(t) = -\frac{1 + \xi_i e^{-i\pi\alpha_i(t)}}{\sin(\pi\alpha_i(t))} \tag{4.40}$$

and g's are the respective vertex couplings. The cross-section is given by:

$$\sigma(s,t,M^2) \underset{s\to\infty}{\sim} \frac{1}{s}\sum_{ij} g^i_{13}(t) g^{j*}_{13}(t) g^i_{2X}(t) g^{j*}_{2X}(t) \eta_i(t)\eta^*_j(t)(\frac{s}{M^2})^{\alpha_i(t)+\alpha_j(t)} \times Disc_{M^2} A(i2 \to j2) \tag{4.41}$$

where $A(i_2 \to j_2)$ is the reggeon-particle scattering amplitude, where the discontinuity is given by:

$$Disc_{M^2} A(i2 \to j2) \underset{M^2\to\infty}{\sim} \sum_k g^k_{22}(0) g_{ijk}(t)(M^2)^{\alpha_k(0)} \tag{4.42}$$

If we restrict our selves to single diffraction, implying that X has same quantum numbers as the other incoming particles, the Reggeons above are more specifically Pomerons.

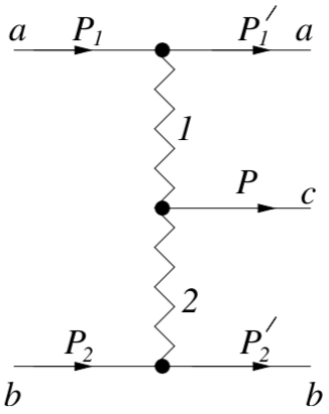

Figure 7 A graphical depiction of Central Exclusive Production. Particles a and b in the momentum configuration (P_1, P_2), undergo a reaction which leaves them in a momentum configuration ($P_1^{'}$, $P_2^{'}$). The remaining phase space is filed by a centrally formed resonance c with momentum P. Figure is taken from Donnachie, S., Dosch, G., Landshoff, P., & Nachtmann, O. [2].

Finally, we reach the main point, namely, Central Exclusive Production (Figure 7), a process of the form: $a(P_1) + b(P_2) \to a(P_1^{'}) + c(P) + b(P_2^{'}))$. There is no restriction on what the particle c might be. We establish the notions of momentum transfer and the final state sub-energy variables [2]:

$$t_1 = (P_1 - P_1^{'})^2 \qquad t_2 = (P_2 - P_2^2)^2 \tag{4.43}$$

$$s_1 = (P_1^{'} + P)^2 \qquad s_2 = (P_2^{'} + P)^2 \tag{4.44}$$

In the case where s_1 and s_2 are both large, but t_1 and t_2 are comparatively small, the process depicted in Figure 7 is the dominant one (compared to e.g. inclusive central production).
Notice that these conditions are equivalent to the ones given above when considering the rapidity topology of diffractive processes. We are ensuring that there is a low momentum interchange in the t-channel and that the outgoing states (almost unchanged from their initial states) are, compared to the intermediate resonance formed (denoted by P), highly energetic. The momenta of the fragments of the intermediate resonance (P) will, therefore, largely be perpendicular to the momenta of the outgoing states (denoted by P_1' and P_2') and almost completely opposite one to another. This is what we call the Double Gap Topology.

Along with the considerations above, one reassures the necessity of observation of the double rapidity gap topology when delving with exclusively centrally produced processes, which contribute the following to the amplitude [2]:

$$\beta_1(t_1)\Gamma(-\alpha_1(t_1))\xi_{\alpha_1(t_1)}\beta_2(t_1)\Gamma(-\alpha_2(t_1))\xi_{\alpha_2(t_2)}f_{12}(\eta) \\ (\frac{s_1}{s_0})^{\alpha_1(t_1)}(\frac{s_2}{s_0})^{\alpha_2(t_2)} \tag{4.45}$$

where $\beta(t)$'s are the Regge-Hadron coupling functions, and ξ_α's are the signature factors. Notice the fixed scale factors s_0 (units of squared mass), which are introduced since it is more convenient to raise a dimensionless quantity to a power. The Γ functions are here due to a rewriting of the Legendre polynomials and the $\sin(\pi l)$ denominators which arise in such calculations. By $f_{12}(\eta)$, we denote the coupling of the 2 Reggeons to the particle P. η is defined as:

$$\eta = \frac{s_1 s_2}{s} \tag{4.46}$$

where it can easily be seen that in our approximation, η is small.

5. Partial Wave Analysis in the Helicity Formalism

In this chapter, we will introduce and derive the helicity basis and introduce partial wave analysis in that framework. I will try to cover all the necessary concepts, without delving in to step by step calculations. The formalism itself can be quite intuitive and transparent given the proper context. This is what I will be aiming to provide, without losing the sense of completeness one would find in a primer. Consider a decay, akin to the dummy process $\alpha \to 1 + 2$, were α is a state of definite spin J. We choose arbitrarily an axis which defines the spin projection m (choose the z-axis).

The amplitude of such a process can, in general, be given in the CMS frame, in the following form [14]:

$$A = \langle \theta, \phi, \lambda_1, \lambda_2 | U | JM \rangle \tag{5.1}$$

where θ and ϕ are the polar angles defined by $\hat{n}$, and U is the time-evolution operator. We will denote the final state by the decay direction w.r.t the spin quantization axis ($\hat{n}$) of α, the magnitude of the momentum and the respective helicities of the fragments. A state defined in such a way is called a two-particle helicity state. The motivation lies with the fact that the rotational invariance of the helicities allows for a set of two-particle basis states $|j, m, \lambda_1, \lambda_2\rangle$ with well defined total angular momentum j, its projection m, and helicities λ_1 and λ_2 of the two particles. From momentum conservation, it can be shown that the decay amplitude of a decayed particle, with a spin projection along the z-axis, is equal to the amplitude for its spin to have a projection $\lambda = \lambda_1 - \lambda_2$ along the decay axis (up to a constant determining the coupling of the initial state to the final state helicities).

5.1 The Rotation Operator $R(\alpha\beta\gamma)$

The rotation operator $R(\alpha\beta\gamma)$ is discussed from an active view of rotations, where it can, in general, be said that an arbitrary rotation $R(\alpha\beta\gamma)$ can always be constructed from three successive rotations, as given in Richman, J. D. [14], as:

$$R(\alpha\beta\gamma) = R_Z(\gamma) R_u(\beta) R_z(\alpha) = e^{-i\gamma J_Z} e^{-i\beta J_u} e^{-i\alpha J_z} \tag{5.2}$$

where we acknowledge the fact that the generator of rotations is the angular momentum operator. Notice the distinction between Z and z, as the former belongs

to the coordinate system assigned to the physical system, and the later to the reference coordinate system (fixed). The axis u is defined by a rotation of the y axis by an angle α. This is visually revealing but not very useful. In this way we are defining rotations w.r.t. an arbitrary, non-fixed frame, rather that w.r.t. a fixed reference frame.

To remedy this shortcoming, we assert that the expectation value of a system consisting of a state vector $|\alpha\rangle$ and an observable Q will remain unchanged under a rotation transformation if the rotated system is given by:

$$|\alpha^{'}\rangle = R\,|\alpha\rangle \tag{5.3}$$
$$Q^{'} = RQR^{\dagger} \tag{5.4}$$

from which it follows that [5]:

$$J_u = R_z(\alpha)J_yR_z^{\dagger}(\alpha) \tag{5.5}$$
$$J_Z = [R_u(\beta)R_z(\alpha)]J_z[R_u(\beta)R_z(\alpha)]^{\dagger} \tag{5.6}$$
$$R(\alpha\beta\gamma) = e^{-i\alpha J_z}e^{-i\beta J_y}e^{-i\gamma J_z} \tag{5.7}$$

Rotation operators of the form $R(\theta) = \exp(-i\theta J)$ introduced above, are in fact the most convenient, irreducible representations of the $SO(3)$ group. One can check this easily by considering that the generators of the group must be anti-symmetric. For a rotation in some $\theta_k\hat{e}_k$ direction we have:

$$R(\theta_k\hat{e}_k)^{-1} = R(-\theta_k\hat{e}_k) = \exp(-\theta_l L_k)$$
$$R(\theta_k\hat{e}_k)^{-1} = R(\theta_k\hat{e}_k)^{T} = \exp(-\theta_l L_k^{T})$$

from which it follows that $L_k^T = -L_k$. This justifies the above-given form with the restriction that the matrix in the exponential must be antisymmetric. Hence, it has only 3 independent elements, i.e. the following form:

$$A = \begin{pmatrix} 0 & a & b \\ -a & 0 & c \\ -b & -c & 0 \end{pmatrix}$$

We can consider how do the aforementioned rotation operators act on elements of the function space $f(\theta,\phi) \in \mathbb{C}_\infty(S_2)$($\mathbb{C}_\infty(S_2)$ is the extended complex space over the unit sphere). This function space is such that $Y_{lm}(\theta,\phi)$ spherical harmonics provide a complete orthonormal basis, and that $\mathbb{C}_\infty(S_2)$ can be represented as [15]:

$$\mathbb{C}_\infty(S_2) = [\{Y_{lm}, l = 0, 1, ...\infty, m = -l, -l+1, ..., l\}] \tag{5.8}$$

where $[\{\}]$ denotes the closure of a set by talking all the possible linear combinations of the elements. This means that the rotation operators are determined completely if we set the transformation behavior of $Y_{lm}(\theta,\phi)$. This transformation behavior is given by the following coefficients [15]:

$$[D(\vec{\theta})]_{l'm';lm} = \int_{S_2} d\Omega Y^*_{l'm'}(\theta,\phi)\exp(-\frac{i}{\hbar}\vec{\theta}\vec{J})Y_{lm}(\theta,\phi) \tag{5.9}$$

These coefficients can be considered as the elements of an infinite dimensional matrix which provides the representation of our rotation operators in the Y_{lm} basis. Consider the set of sub-spaces $\mathbb{X}_l$ of $\mathbb{C}_\infty(S_2)$:

$$\mathbb{X}_l = [\{Y_{lm}, m = -l, -l+1, ..., l\}] \quad , l = 0, 1, 2, ... \tag{5.10}$$

where we claim rotational invariance under rotation operators, as introduced above, and that all $\mathbb{X}_l$'s form the lowest dimensional sets $\mathbb{X}_l$ which obey $\mathbb{C}_\infty(S_2) = \cup_{l=1}^{\infty}\mathbb{X}_l$. We notice that these rotation operators can be written in the following form:

$$\exp(\frac{-i}{\hbar}\vec{\theta}\vec{J}) = \sum_{n_1,n_2,n_3} c_{n_1,n_2,n_3} J_+^{n_1} J_-^{n_2} J_3^{n_3} \tag{5.11}$$

where by considering individually the action of J_+, J_- and J_3 operators on spherical harmonics, one can conclude that these operatoes leave the $\mathbb{X}_l$ sub-spaces invariant, and that only the $l = l^{'}$ terms of the $D(\vec{\theta})_{l'm';lm}$ transformations contribute.

We can order the basis according to the partitioning (5.13) of the $\mathbb{C}_\infty(S_2)$ space, where the matrix representation of the $D(\vec{\theta})_{l'm';lm}$ assumes a block-diagonal form:

$$A = \begin{pmatrix} \boxed{1\times 1} & & & \\ & \boxed{3\times 3} & & \\ & & \ddots & \\ & & & \boxed{(2l+1)\times(2l+1)} \end{pmatrix} \tag{5.12}$$

This is a more general demonstration, which shows an irreducible representation of the $D(\vec{\theta})_{l'm';lm}$ transformation. Hence, it indicates that the rotation operators as introduced are a part of an irreducible representation of $SO(3)$ (this can be easily seen from $[R, J^2] = 0$) [14].

5.2 Rotation of Angular Momentum Eigenstates

Since $[R, J^2] = 0$, we maintain that angular momentum eigenstates transform irreducibly under rotations. The rotation operator $R(\alpha\beta\gamma)$ acts on a angular

momentum eigenstate as [5]:

$$R(\alpha\beta\gamma)\,|jm\rangle = \sum_{m=-j}^{j} D^{j}_{m^{'}m}(\alpha\beta\gamma)\,|jm^{'}\rangle \tag{5.13}$$

We can use Eq. (5.7) to express the Wigner-D functions $D^{j}_{m^{'}m}$, in the following form:

$$D^{j}_{m^{'}m} = e^{-i\alpha m^{'}} d^{j}_{m^{'}m}(\beta) e^{-i\gamma m} \tag{5.14}$$

where the matrix element:

$$d^{j}_{m^{'}m}(\beta) = \langle jm^{'}|e^{-i\beta J_y}|jm\rangle$$

is given by the d-Wigner formula:

$$\begin{aligned} d_{m^{'}m}(\beta) = \sum_{n}\{&\frac{(-1)^n[(j+m)!(j-m)!(j+m^{'})!(j-m^{'})!]^{1/2}}{(j-m^{'}-n)!(j+m-n)!(n+m^{'}-m)!n!} \\ &\times(\cos(\frac{\beta}{2}))^{2j+m-m^{'}-2n}(-\sin(\frac{\beta}{2}))^{m^{'}-m+2n}\} \end{aligned} \tag{5.15}$$

The sum necessarily includes only integers for which the factorial arguments remain non-negative. These functions are clearly real. We state several useful symmetry relations for the small d-Wigner functions, for the sake of completeness.

$$d^{j}_{m^{'}m}(-\beta) = (-1)^{m^{'}-m} d^{j}_{m^{'}m}(\beta) \tag{5.16}$$

$$d^{j}_{m^{'}m}(-\beta) = d^{j}_{mm^{'}}(\beta) \tag{5.17}$$

$$d^{j}_{m^{'}m}(\beta) = (-1)^{m^{'}-m} d^{j}_{mm^{'}}(\beta) \tag{5.18}$$

These can be used to obtain some useful properties of the D-Wigner functions:

$$D^{j}_{mm^{'}}(0,\beta,0) = D^{j}_{m^{'}m}(0,-\beta,0) \tag{5.19}$$

$$D^{j}_{m^{'}m}(\alpha\beta\gamma) = D^{j}_{mm^{'}}(\gamma,-\beta,\alpha) \tag{5.20}$$

as well as the orthogonality relation:

$$\begin{aligned} \int_0^{2\pi}\int_0^{2\pi}\int_0^{\pi} \sin(\beta) d\beta [D^{j*}_{mn}(\alpha\beta\gamma) D^{j^{'}}_{m^{'}n^{'}}(\alpha\beta\gamma)] = \\ \frac{8\pi^2}{2j+1}\delta_{mm^{'}}\delta_{nn^{'}}\delta_{jj^{'}} \end{aligned} \tag{5.21}$$

5.3 Relativistic Two-Particle States in the Helicity Frame

Let's introduce the necessary parts in order to construct the relativistic two-particle states in the helicity frame. A canonical state representation of a single particle with definite spin j, spin projection m, and momentum $\vec{p}$ is given by [5]:

$$\begin{aligned} |\vec{p}, jm\rangle = |\phi, \theta, p, jm\rangle &= U[L(\vec{p})]\,|jm\rangle \\ &= U[\dot{R}(\phi,\theta,0)]U[L_z(p)]U^{-1}[\dot{R}(\phi,\theta,0)]\,|jm\rangle \end{aligned} \tag{5.22}$$

where $L(\vec{p})$ is the Lorentz boost and $U[L(\vec{p})]$ represents the corresponding unitary operator which can act on single particle states. Rotation $\dot{R}(\phi,\theta,0)$ aligns the z-axis with the momentum direction.

The important insight here is that canonical single particle states transform under rotations in the same way as non-relativistic, resting particle states would.

$$\begin{aligned} U[R]\,|\vec{p}, jm\rangle =& U[R\dot{R}]U[L_z(p)]U^{-1}[R\dot{R}]U[R]\,|jm\rangle \\ &= \sum_{m'} D^{j}_{m'm}(R)\,|R\vec{p}, jm'\rangle \end{aligned} \tag{5.23}$$

We define a single particle state in the helicity frame as [5]:

$$\begin{aligned} |\vec{p}, j\lambda\rangle = |\phi, \theta, p, j\lambda\rangle &= U[L(\vec{p})]U[\dot{R}(\phi,\theta,0)]\,|j\lambda\rangle \\ &= U[\dot{R}(\phi,\theta,0)]U[L_z(p)]\,|j\lambda\rangle \end{aligned} \tag{5.24}$$

where we acknowledge that it is equivalent to firstly boost the particle state at rest, and subsequently rotate it so that we align the z-axis with the boost direction, or firstly rotate the system and then boost it.The helicity λ is a rotational invariant in the helicity frame, and is most importantly unaffected by pure Lorentz boosts.

As stated in Chung, S. U. [5], the two particle state in the canonical basis is given by:

$$|\phi\theta m_1 m_2\rangle = aU[L(\vec{p})]\,|s_1 m_1\rangle\, U[L(-\vec{p})]\,|s_2 m_2\rangle \tag{5.25}$$

where a is a normalization constant, and particle spin is denoted by s_1 and s_2 respectively. We can relate single spin states to states of total spin, via the standard Clebsch-Gordan coefficients, and introduce fixed angular momenta by integrating out the Ω space angle dependence (by means of the $Y_l^m(\Omega)$ spherical harmonics).

From here, one can consider states of total angular momentum, where we note that l and s are rotational invariants (for any rotation R, which takes $\Omega = (\theta, \phi)$ in to $R^{'} = R\Omega$). The relation of one-particle spin states to the states of total angular momentum are analog to the non-relativistic $L - S$ coupling [4].

Building on the discussion above, we define the helicity basis two-particle states as [5]:

$$\begin{aligned} |\phi\theta\lambda_1\lambda_2\rangle &= aU[\dot{R}]\{U[L_z(\vec{p})]\,|s_1\lambda_1\rangle\,U[L_{-z}(\vec{p})]\,|s_2 - \lambda_2\rangle\} \\ &\equiv U[\phi, \dot{\theta}, 0]\,|00\lambda_1\lambda_2\rangle \end{aligned} \tag{5.26}$$

where a is once again a normalization constant. Two-particle eigenstates of definite total angular momentum can be constructed and given in the following [4]:

$$|JM\lambda_1\lambda_2\rangle = N_J \int d\Omega D^{J*}_{M\lambda}(\phi, \theta, 0)\,|\phi\theta\lambda_1\lambda_2\rangle \tag{5.27}$$

where $\lambda = \lambda_1 - \lambda_2$. Note that λ_1 and λ_2 are rotational invariants (arbitrary rotation).

5.4 Helicity Amplitudes

The transition amplitude for the decay of a particle α, with well defined total angular momentum and spin (along with its projection), into two daughter particles β and γ can be constructed in both the canonical and helicity frame. For our purposes, it is really only interesting to demonstrate the helicity amplitudes, but for the sake of completeness, I state both of them. The canonical transition amplitude as in Peters, K. [4], is given by:

$$A^{JM}_{m_\beta m_\gamma} \equiv \sum_{L,S,m_L,m_S} \sqrt{4\pi} a^J_{LS}(Lm_L Sm_S|JM)(\beta m_\beta \gamma m_\gamma|Sm_S)Y^L_{m_L}(\Omega) \tag{5.28}$$

where the partial decay amplitudes a^J_{LS} (L denotes the orbital angular momentum quantum number, while S denotes spin) are given by:

$$a^J_{LS} \equiv \sqrt{\frac{4\pi}{\rho}}\,\langle JMLS|JM\rangle \tag{5.29}$$

The helicity transition amplitude is given by [4]:

$$A^{JM}_{\lambda_\beta\lambda_\gamma} = N_j f^J_{\lambda_\beta\lambda_\gamma} D_{M,\lambda_{s'}-\lambda_{t'}}(\Omega) \tag{5.30}$$

where the helictiy amplitudes $N_j f^J_{\lambda_\beta \lambda_\gamma}$ are given by:

$$N_j f^J_{\lambda_\beta \lambda_\gamma} = \sqrt{\frac{4\pi}{\rho}(2J+1)} \langle JM\lambda_s m_t|T|JM\rangle \tag{5.31}$$

The main point to see here is that we are expressing the amplitudes in term of a superposition of spherical functions of a different type, weighted by the decay matrix element. For this type of processes, the helicity basis is a convenient choice for the decay amplitudes. It allows us to obtain expressions, easily comparable to the experimentally obtainable cross-sections parametrized in terms of angular distributions.

More explicitly, the angular distributions are obtainable once we specify the population of $2J+1$ sub-states of the initial state, by an initial spin density matrix, giving an expression for the angular intensities as:

$$I(\theta,\phi)_{\lambda\lambda'} = Tr(\rho_f) = Tr(A^{JM}_{\lambda_\beta\lambda_\gamma}(\phi,\theta)\rho_i A^{JM'*}_{\lambda_{\beta'}\lambda_{\gamma'}}(\phi,\theta)) \tag{5.32}$$

where the summation is implicitly constrained to $\lambda = \lambda_\beta - \lambda_\gamma$ and $\lambda' = \lambda_{\beta'} - \lambda_{\gamma'}$. Factors multiplying the D-Wigner functions in Eq. (5.31) basically trickle down to complex fit parameters, which get optimized by PWA on a set basis of partial waves. However, due to symmetry relations and conservation laws (for an extensive list and discussion refer to Chung, S. U. [5]), some amplitudes may vanish. This can significantly reduce the number of free fit parameters in PWA (which is usually quite important due to the whole procedure being computationally intensive).

5.5 Multiple Decay Chains (The Isobar Model)

In Section 4.4, we have introduced and defined the concept of an initial spin configuration in the form of a density matrix. This is something which is generally quite hard to obtain, and more often than not, we are talking of unpolarised particle beams. This means that there isn't a preferred spin configuration, which reduces the spin density matrix to a normalized unity matrix. This tallies quite a few implications.
Consider the amplitudes given by Eq. (5.30) and their relation to the corresponding cross section given by Eq. (5.32). All the information of the distribution of angle ϕ is contained in the complex exponential, which results in flat angular distributions of ϕ for all symmetric density matrices without off-diagonal elements, as in relation (5.32). From the symmetry relations for the D-Wigner functions, positive and negative angular momentum projections states cancel each other completely, if not mixed by the density matrix to produce interference. This results in flat θ distributions (in actual simulations, when considering phase space distribution, we actually mean flat in $\cos(\theta)$).

It is therefore of paramount importance for PWA to consider a multiple decay chain since for any purely unpolarised beam, it is impossible to get a non-trivial angular distribution for a single decay. However, intermediate processes that are contributing to a decay chain, can in some cases be interpreted as having a polarized beam for a single decay, and therefore provide information which can essentially completely be represented by a spin density matrix (in addition to additional amplitudes which contribute in a fashion described below). This may, and usually does, produce a density matrix such that one does obtain non-flat angular distributions.
In PWA, we approach the decay amplitude of a resonance with more than two final particles as a product of successive, two-body decay amplitudes. I will give the relations in a slightly cumbersome way, which are, in my opinion, quite useful for computational implementation. Instead of a generic $A \to B + C$, we consider $B \to B_1 + B_2$ and $C \to C_1 + C_2$. The transition amplitude for this complete chain is given by [16]:

$$\begin{aligned} f_T &= [f(B) \otimes f(C)] f(A) \\ &= \sum_{\lambda(B)\lambda(C)} \{ f_{\lambda(B_1)\lambda(B_2),\lambda(B)} \otimes f_{\lambda(C_1)\lambda(C_2),\lambda(C)} \} f_{\lambda(B)\lambda(C),\lambda(A)} \end{aligned} \tag{5.33}$$

where $\otimes$ denotes the tensor product and the f amplitudes are given by (5.30). Note that the implicit three pairs of (θ, ϕ) are each defined in different frames, namely, rest frames of the corresponding decays (this might be the Helicity frame

or something like the Gottfried-Jackson frame [17]. In this chapter we are exclusively dealing with the Helicity frame.)

5.6 Simulation Study: $f_2(1270) \to \pi^+\pi^-$

We dediceated significant time to implement and demonstrate angular distributions constituents in PWA. Therefore, we chose some cases which seem to be well represented in primers (e.g Peters, K. [4]), one of which is, as the title suggests, $f_2(1270) \to \pi^+\pi^-$ decay.
Due to the quantum numbers (f_2 initial state has $I^G(J^{PC}) = 0^+(2^{++})$, while the pions are $I^G(J^{PC}) = 1^-(0^{-+})$), intrinsic parity of the f_2 is even and $l = 2$, while the total s spin is zero, resulting in $\lambda = 0$ and $J = 2$. This amounts to us having only one amplitude, namely [4]:

$$\begin{aligned} A_{00}^{2M}(\theta,\phi) &= N_2 f_{00}^2 D_{M0}^{2*}(\theta,\phi) \\ &= N_2 f_{00}^2 \begin{pmatrix} d^2_{-20}(\theta)e^{-2i\phi} \\ d^2_{-10}(\theta)e^{-i\phi} \\ d^2_{00}(\theta) \\ d^2_{10}(\theta)e^{i\phi} \\ d^2_{20}(\theta)e^{2i\phi} \end{pmatrix} \end{aligned} \tag{5.34}$$

where $N_2 f_{00}^2$ is a constant given by:

$$N_2 f_{00}^2 = \sqrt{5}(2000|00)(0000|00)a_{20} = \sqrt{5}a_{20}$$

Initially, we set the density matrix to a generic, normalized identity matrix, as we have no information on the possible chains leading up to the decay or to the initial spin configuration. However, what we have done is manually set the density matrices in such a way to see what the "building blocks" of the angular distributions look like and what can we expect for angular distributions. This is achieved by "turning off" all d-Wigner contributions, except for one at a time. The scaling factors are irrelevant for this purpose and have not been included in the implementation. As a test for our code and understanding of the procedure, we made pure PWA theoretical presumptions, plotted the resulting angular distributions, and then superimposed these with actual data corresponding to out assumptions.

For this purpose, we used EvtGen [18], a software of the BaBar collaboration. This is a robust Monte-Carlo Generator for B-Physics with multiple useful modes of operation (e.g PHSP for phase space simulations). We made extensive use of its HELAMP mode, which simulates decays directly from the transition amplitudes. These have to be given a priori with relative weights (something one would

get if we define a production mechanism e.g a chained decay) [18]. The software allowed us to set the spin density matrices directly, without having to construct any chains in both the canonical and helicity frames.

Because EvtGen understands phase space and observes conservation laws, the decays are generated flat in $\cos(\theta)$. In order to be able to match the PWA predictions with the simulated data, we had to include the Jacobian (extra $\sin(\theta)$ factor multiplying the intensity) from the coordinate transformation. The corresponding intensities in θ obtained are shown in Figures 8 to 12.

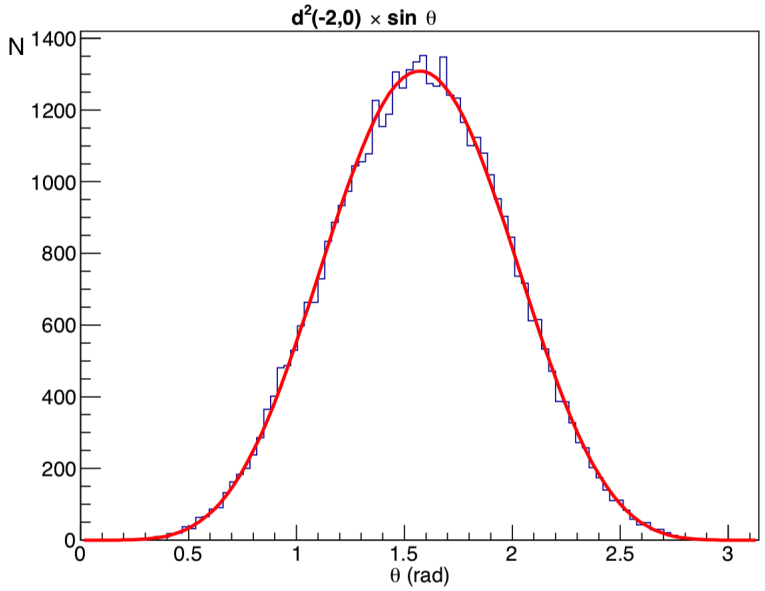

Figure 8 A superposition of EvtGen simulated angular distribution in θ(blue) against theoretical values represented by the corresponding d-Wigner function(red) and the Jacobian from the coordinate transformation.

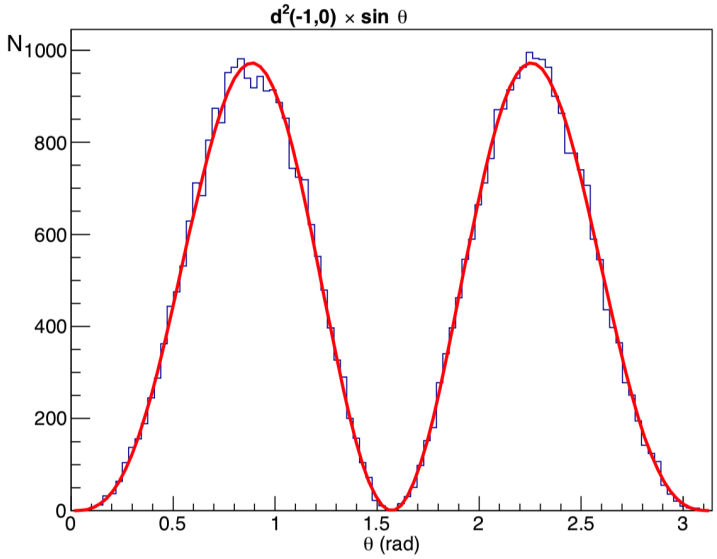

Figure 9 A superposition of EvtGen simulated angular distribution in θ(blue) against theoretical values represented by the corresponding d-Wigner function(red) and the Jacobian from the coordinate transformation.

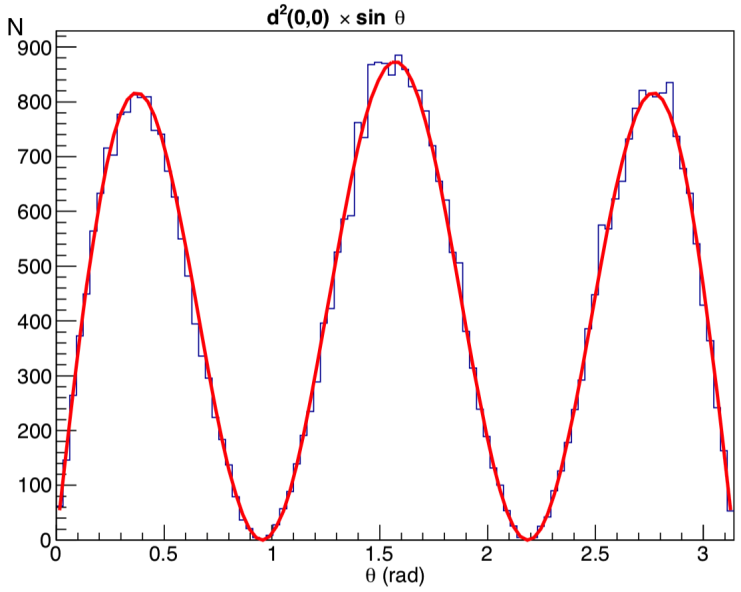

Figure 10 A superposition of EvtGen simulated angular distribution in θ(blue) against theoretical values represented by the corresponding d-Wigner function(red) and the Jacobian from the coordinate transformation.

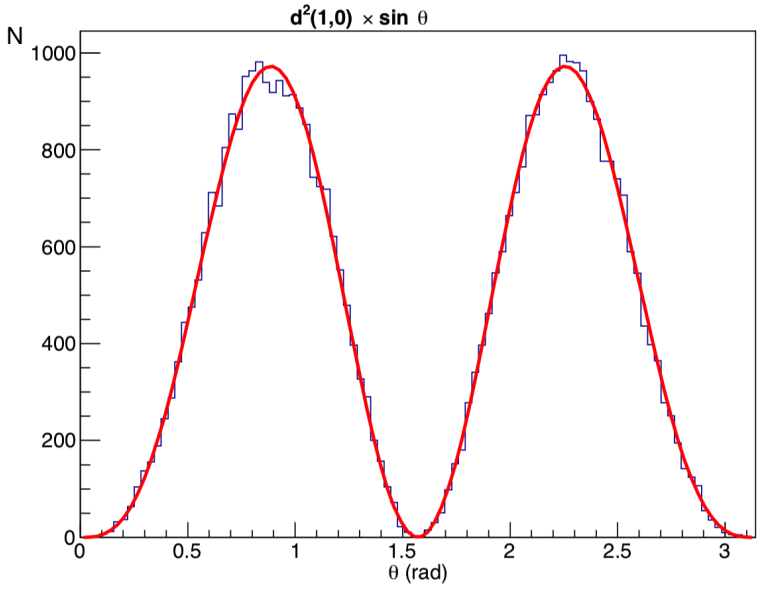

Figure 11 A superposition of EvtGen simulated angular distribution in θ(blue) against theoretical values represented by the corresponding d-Wigner function(red) and the Jacobian from the coordinate transformation.

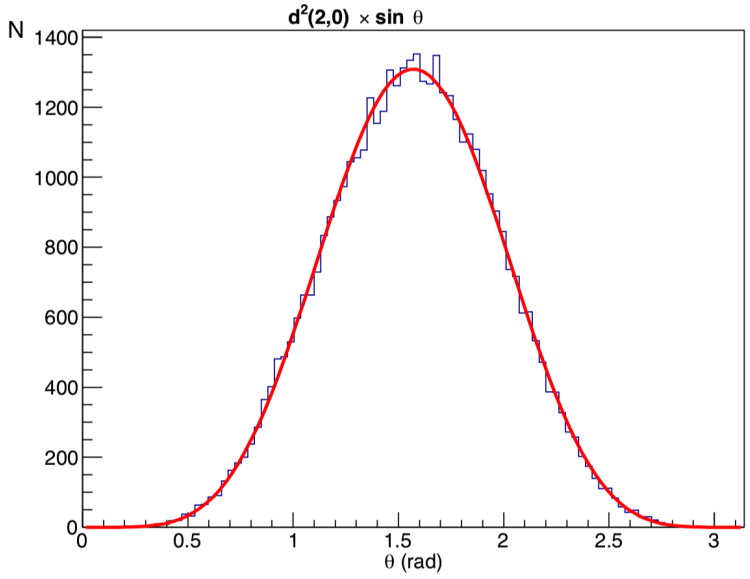

Figure 12 A superposition of EvtGen simulated angular distribution in θ(blue) against theoretical values represented by the corresponding d-Wigner function(red) and the Jacobian from the coordinate transformation.

5.7 Simulation Study: $\rho_0 \rightarrow \pi^+\pi^-$

In this simulation study, we consider $\rho_0(770)$, which is a vector resonance ($I^G(J^{PC}) = 1^+(1^{--})$). This allows for only one possible amplitude, since $s = 0$ and parity conservation implies that $j = l = 1$. As in the example above, the actual helicity amplitude, which is a constant factor serving the purpose of weighting the relative amplitude contributions, is irrelevant. The amplitude is given by:

$$\begin{aligned} A_{00}^{1M}(\theta,\phi) &= D_{M0}^{1*}(\theta,\phi) \\ &= \begin{pmatrix} d_{-10}^{1}(\theta)e^{-i\phi} \\ d_{00}^{1}(\theta) \\ d_{10}^{1}(\theta)e^{i\phi} \end{pmatrix} \end{aligned} \tag{5.35}$$

We manipulated the spin density matrix again in such a way to obtain individual contributions from the D-Wigner functions and superposed them with the EvtGen simulated data. The corresponding intensities in θ are shown in Figures 13 to 15.

Let's see how would the predictions from this example change if we were considering it as a part of a decay chain, namely ${}^3S_1(\bar{p}p) \rightarrow \rho_0\pi^0, \rho_0 \rightarrow \pi^+\pi^-$. I revert here to the notation used in the Amsler, C., & Bizot, J. C. [16], and make appropriate analogies where deemed necessary. As discussed in Amsler, C., & Bizot, J. C. [16], the only allowed angular momentum for the $\rho\pi$ system is $l = 0$. Since spin is limited to $s = 1$, once again, the helicity amplitude is unity, and the transition amplitude is given by:

$$f_{\lambda_1 0,M}(\theta,\phi) = \begin{pmatrix} D_{11}^{1} & D_{10}^{1} & D_{1-1}^{1} \\ 0 & 0 & 0 \\ -D_{-11}^{1} & -D_{-10}^{1} & -D_{-1-1}^{1} \end{pmatrix} \tag{5.36}$$

The total transition amplitude f_T, by respecting the rule (5.33), is given by:

$$f_T = \sum_{\lambda_1} f_{00,\lambda_1}(\theta^{'},\phi^{'}) f_{\lambda_1 0,M}(\theta,\phi) \tag{5.37}$$

where $\theta^{'}$ and $\phi^{'}$ are the angles describing π^- in the rest frame of its mother.
Here we have another set of amplitudes, presenting some combinations of D-Wigner functions, which will (for a normalized unity spin density matrix, e.g. unpolarised beam) give an angular distribution in θ of the form $\sin^2\theta$ [16]. The production mechanism might, however, introduce a polarization which significantly modifies this prediction.

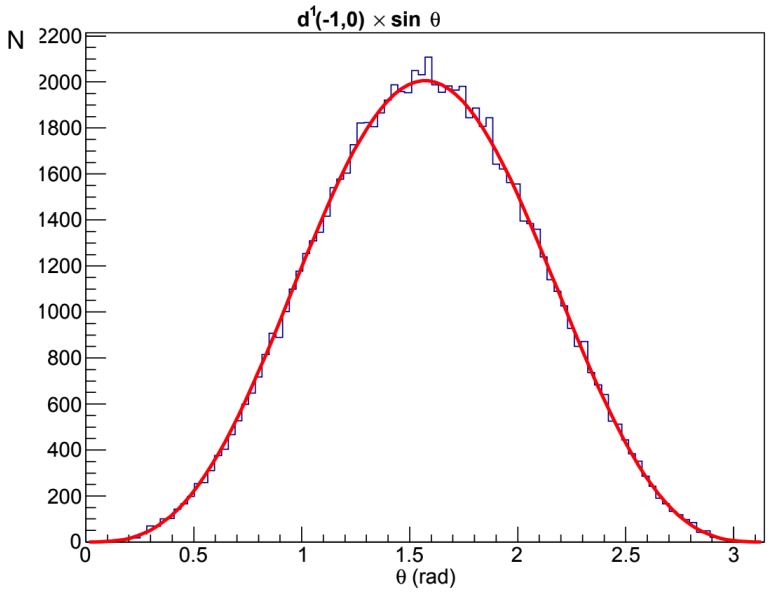

Figure 13 A superposition of EvtGen simulated angular distribution in θ (blue) against theoretical values represented by the corresponding d-Wigner function (red) and the Jacobian from the coordinate transformation.

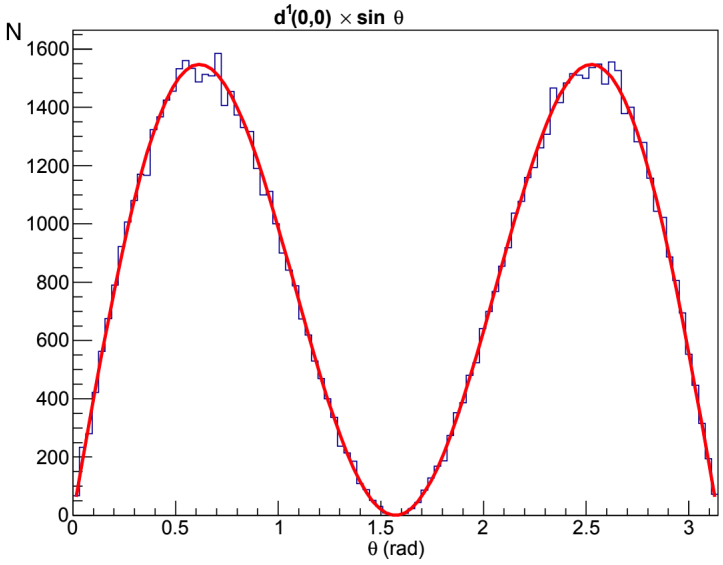

Figure 14 A superposition of EvtGen simulated angular distribution in θ (blue) against theoretical values represented by the corresponding d-Wigner function (red) and the Jacobian from the coordinate transformation.

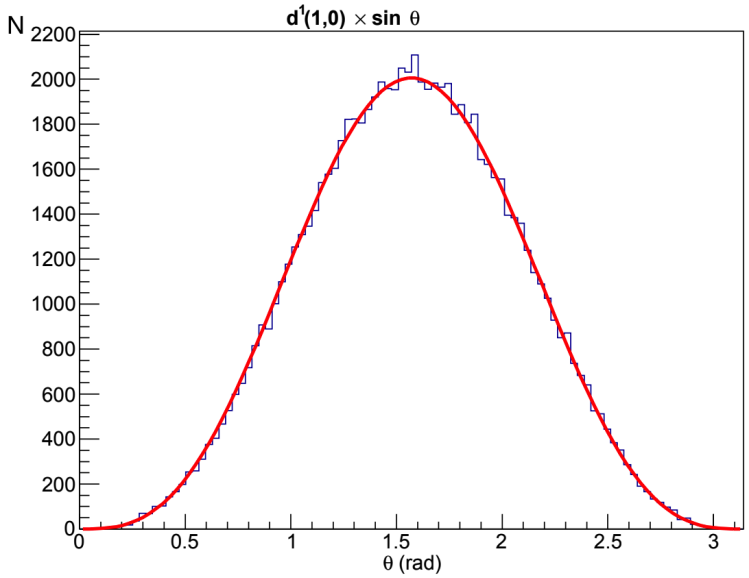

Figure 15 A superposition of EvtGen simulated angular distribution in θ (blue) against theoretical values represented by the corresponding d-Wigner function (red) and the Jacobian from the coordinate transformation.

6. Resonances in Partial Wave Analysis

Right off the bat, we must highlight the fact that we only considered the angular part of the full transition amplitude for a resonance decay till now. The assumption we made behind the scenes is that the amplitude can be separated into a purely angular part, as discussed in Chapter 3, and into a purely mass dependent part.
As far as the purely angular part is concerned, how one uses PWA in reproducing data hasn't really been discussed. The main point of concern is the sheer number of partial waves (set of quantum numbers $\{I^G J^{PC} mLls\}$, which translates to amplitudes) which might be possible. Consider a final multiparticle state, consisting of π^+, π^- and π^0. This system has a G-party of -1, and let us take $I \leq 1$. This allows for I^G states to be $I^G = 0^-$ (isoscalar, $C = -1$), and $I^G = 1^-$ (isovector, $C = +1$) [19].

Which partial waves to include in the PWA? One starts with a set of J and m quantum numbers. For a two-particle decay, the number of possible resonant states is $\sum_J (2J + 1)$. For definite spins of final particles, dented by s_1 and s_2, there can be $\sum_{J,s_1,s_2} (2J + 1)(2s_1 + 1)(2s_2 + 1)$ final states. If we have spinless final states, this leaves us with $\sum_l (2l + 1)$ partial waves [5].

For a decay chain, one first needs to decide how to express the final states in term of the isobar model. In practice, one must consider any two particle combination of the final states, which might correspond to a known resonance. We apply the PWA formalism for each node recognized in the decay chain, on a set of allowed partial waves. This is similar to what has been demonstrated in Chapter 3, where we have left out the mass-dependent factor Q_{ls} which comes from the propagation of the isobar. In general, Q_{ls} is a dynamical parameter dependent on the isobar, the masses of the daughter particles, and the interfering and overlapping resonances [19].

A good approach to define a set of partial waves is to start with a large number of them and reduce their number iteratively. We discriminate the partial waves which don't contribute to the fit. However, there is no definite way of going about this except for just trying different combinations until one obtains the minimal set of amplitudes which represent the data (ideally a unique one). For a demonstration of this and further discussion, refer to Chapter 7.

6.1 Mass-independent fit in PWA

In terms of hadron physics at the ALICE detector on the LHC in CERN, we obtain data in the form of energy and momentum measurements of the charged final states. Assuming that we can perfectly backtrack the final states to their respective resonances, and these are non-overlapping and significant, by means of invariant-mass analysis, one should reproduce a Breit-Wigner shape. A Breit-Wigner is fully determined by its mass and width (more on this in the next Chapter). This is a depiction of cross-sections, in terms of mass. They can be expressed in the partial wave basis, as introduced in Chapter 4, with an additional Q_{ls} mass-dependent function. The point of mass-independent fitting is that, for each mass bin of data, these Q_{ls} functions are of no relevance.

To fit the model, we used the extended likelihood fit, in the following form:

$$\ln \mathcal{L} = \sum_{i=1}^{N} \ln[\mathcal{P}(\vec{x_i}, \vec{a})] - \mathcal{N} \tag{6.1}$$

where $\mathcal{P}(\vec{x_i}, \vec{a})$ represents the extended probability space ($\mathcal{P}(\vec{x_i}, \vec{a}) = \mathcal{N} p(\vec{x_i}, \vec{a})$), $p(\vec{x_i}, \vec{a})$ is the probability of obtaining an event from the set of parameters $\vec{x_i}$ from a model described by a set of parameters $\vec{a}$.). $\mathcal{N}$ is the expected number of events to be observed in the full phase space determined by a mass range ΔM and t-channel momentum range Δt. We obtain Δt by means of a Monte-Carlo simulation of the detector and a flat phase space simulation of the reaction. We associate $\mathcal{P}(\vec{x_i}, \vec{a})$ with the intensity ($\mathcal{P}(\vec{x_i}, \vec{a}) = I(\tau_i)$), given in the partial wave basis as in Eq. (5.32), where the normalised probability is given by:

$$p(\vec{x_i}, \vec{a}) = \frac{I(\tau_i)}{\mathcal{N}} = \frac{I(\tau_i)}{\int I(\tau_i)\nu(\tau)d\tau} \tag{6.2}$$

where $\nu(\tau)$ is the acceptance, which will be set to either one or zero, dependent on the MC simulation of the detector (detector are not equally as effective for all energies and angles, which has to be taken into account.). As the direct analysis of the data is in terms of invariant-mass analysis, the binning is done with respect to mass only. Therefore, we introduce a Regge theory-based model for the t-channel dependence correction in the MC simulation. Minimization of Eq. (6.1) determines the relative weights (e.g. helicity amplitudes) for the partial waves determined to be present in a mass bin [19].

6.2 Breit-Wigner model in PWA (Mass-dependent fit)

In general, physical states occur as poles of the S-Matrix either on the physical sheets (bound states) or on the nonphysical sheets (resonances) [20]. As previously suggested, resonance properties can be represented by a Breit-Wigner parametrization. However, this parametrization violates the unitary and analyticity of the S-matrix, which in certain cases requires more sophisticated parameterizations (e.g overlapping resonances with coupled decay channels).
One usually decomposes the physical amplitudes M into a pole and non-pole part, which might be interpreted as background in a certain sense. This splitting is, however, not unique. Only the pole position of the resonance X in the complex plane s and its residue are unique. One often uses the following relation for the position of the resonance in the complex s plane:

$$\sqrt{s_X} = M_X - i\Gamma_X/2 \tag{6.3}$$

where M_X and Γ_X are the mass and the width of the resonance X. For N resonances in a particular channel, the pole part of the amplitude is given by [20]:

$$\mathcal{M}_{ba}^{pole}(s) = \gamma_b(s)[1 - V^X(s)\sum(s)]^{-1}_{bc} V^X_{ca}(s)\gamma_a(s) \tag{6.4}$$

where $V^X(s)$ matrices are given such that:

$$V^X_{ab}(s) = -\sum_{n=1}^{N} \frac{g_{nb}g_{na}}{s - M_n^2} \tag{6.5}$$

and γ_a denotes the normalised vertex function. The self-energy is denoted with $\sum_a$, while g_{na} stands for the coupling of a resonance X_n to channel a, and M_n is its mass parameter. For a isolated resonance (6.4), as given in Patrignani, C., & Particle Data Group. [20], we have:

$$\mathcal{M}_{pole}(s)_{ba}|_{N=1} = -\gamma_b(s)\frac{g_b g_a}{s - \hat{M_X}(s)^2 + i\sqrt{s}\Gamma^X(s)_{tot}}\gamma_a(s) \tag{6.6}$$

with:

$$\hat{M}_x(s)^2 = M^2 + \sum_c g_c^2 \Re(\sum_c) \tag{6.7}$$

$$\Gamma^X_c(s) = \frac{(2\pi)^4}{2\sqrt{s}} g_c^2 \int d\phi_c |\gamma_c|^2; \qquad \Gamma^X(s)_{tot} = \sum_c \Gamma^X_c(s) \tag{6.8}$$

Note that $\int d\Phi$ denotes the Lorentz-invariant integral (for details refere to Peskin, M. E. [21]) . For an isolated resonance, reasonably removed from all the relevant thresholds, one can substitute $\Gamma_X(s)_{tot}$ with a constant Γ_{BW}, and absorb the real part of the self-energy function into the mass parameter. This reduces Eq. (6.6) to:

$$\mathcal{M}_{ba}^{pole}|_{N=1} = \frac{g_b g_a}{s - M_{BW}^2 + i\sqrt{s}\Gamma_{BW}} \tag{6.9}$$

For a narrow resonance, it is not uncommon to replace $\sqrt{s}$ with M_{BW}. Note that the Breit-Wigner parameters do not necessarily correspond to the pole parameters as given in (6.3). In the neighborhood of the relevant thresholds, one needs to replace Γ_{BW} with the function $\Gamma(s)$. The exact parametrization, as found in Bevan, A., & Wilson, F. [22], which is the form we have implemented in our programs, is as follows:

$$\mathcal{M}^{pole}|_{N=1} = \frac{m_0\Gamma_0}{m_0^2 - m^2 - im\Gamma(m)} \tag{6.10}$$

where m_0 is the resonance mass, Γ_0 is the resonance width (lifetime), and $\Gamma(m)$ is given by:

$$\Gamma(m) = \Gamma_0 \frac{m_0}{m} (\frac{\rho(m)}{\rho(m_0)})^{2J+1} \frac{F(R\rho(m))}{F(R\rho(m_0))} \tag{6.11}$$

where R is the interaction radius (detector specific), and $\rho(m)$ is given by:

$$\rho(m) = \frac{m}{2}(1 - \frac{(m_a + m_b)^2}{m^2})^{1/2}(1 - \frac{(m_a - m_b)^2}{m^2})^{1/2} \tag{6.12}$$

and the functions F are the spin-dependent Blatt-Weisskopf form factors.
This is going to serve as our model for the remaining fit parameters Q_{ls} in the mass-dependent fit, which we have conveniently neglected till now. The mass-independent fitting procedure has provided us with relative weights for partial waves in each mass bin. We impose a Breit-Wigner mass distribution, which will determine the relative mass weights.

This might be more intuitive to think about when one considers that a Breit-Wigner (6.10) can be represented in terms of a width and a phase shift as follows [19]:

$$\mathcal{M}^{pole}|_{N=1} = \frac{\Gamma_0}{\Gamma(m)} e^{i\delta} \sin(\delta) \tag{6.13}$$

where we introduce the phase shift such that:

$$cos\delta(m) = \frac{m_0^2 - m^2}{m_0^2} \qquad sin\delta(m) = \frac{m_0\Gamma(m)}{m_0^2}$$

and for the moment, we forget about the centrifugal barrier effects. As a small side note, this formulation of the Breit-Wigner proved quite hard to implement, because one needs to use an inverse trigonometric function to extract parameters. This is problematic since it involves branch cuts, and one needs to introduce additional complex sheets, which is computationally quite cumbersome. Additional degrees of freedom come from the production phase for the l wave (mass independent) and a constant scaling factor. A single wave phase is completely arbitrary for any wave, and therefore must be considered with respect to another wave, as only the phase difference can contain physical information. This difference in phase manifests itself as interference in the mass distribution.
The phase difference between 2 partial waves l_1 and l_2, can be extracted by the following relation [19]:

$$\Delta\mathcal{M}^{pole}_{l_1,l_2}|_{N=1} = arctan[\frac{\Im(\mathcal{M}^{pole}_{l_1}|_{N=1}\mathcal{M}^{*pole}_{l_2}|_{N=1})}{\Re(\mathcal{M}^{pole}_{l_1}|_{N=1}\mathcal{M}^{*pole}_{l_2}|_{N=1})}] \tag{6.14}$$

This comes as a very important effect when dealing with overlapping resonances coupled to the same channel (partial wave) or when a single resonance is coupling to multiple decay channels (significantly more complicated and can't be tackled in this parametrization at all).
The former case can sometimes be described by a naive addition of Breit-Wigner's, but such an approach is generally wrong, as it will often result in a violation of unitarity and analyticity of the S-Matrix [20]. Clearly, since Breit-Wigner amplitudes are essentially complex numbers, the addition of such amplitudes is still in the complex space. Hence, the values of the amplitudes should lie exclusively on a unit circle in the complex plane. The violation of unitarity and its "degree" are most effectively demonstrated by means of Argand Diagrams, where we plot the real part of the amplitudes against its imaginary part. If unitarity is not violated, one should see exclusively a unit circle in the complex plane.
In order to observe and get familiar with this behavior, we considered a well-documented case, were two resonances couple to the $J^{PC} = 0^{++}$ channel (PC quantum numbers not really relevant for this discussion). We took two pairs of resonances, where one pair represents the case where the resonances are well above their respective thresholds, and the overlap should be small.
For the second pair, we expect interference effects. The cases in question are:

$$f_0(1200, \Gamma_0 = 100) \qquad f_0(1800, \Gamma_0 = 100)$$
$$f_0(1350, \Gamma_0 = 300) \qquad f_0(1500, \Gamma_0 = 100)$$

The results from the Breit-Wigner model are shown in Figures 16 to 19. The intensities in Figures 16 to 19 are obtained by simple addition of the Breit-Wigner amplitudes, calculated for each resonance respectively. Notice how unitarity is violated in both cases, even if the resonances are relatively well separated. In the next section, we will demonstrate that once one ensures compatibility with the unitary and analyticity of the S-Matrix, even the interference line shapes coming from the Breit-Wigner model are starkly wrong. A solution to this issue comes in the form of the K-Matrix formalism, as will be discussed in the next section.

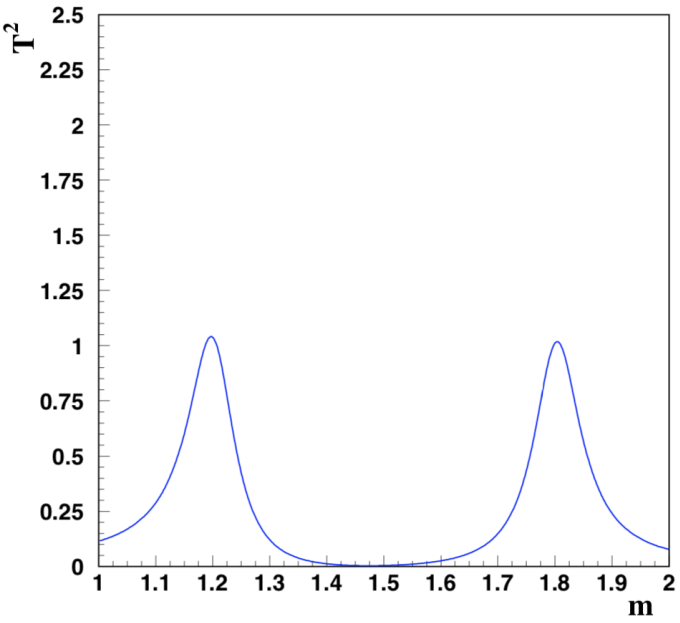

Figure 16 The Breit-Wigner model for the case where two resonances couple to the $J^{PC} = 0^{++}$ channel with resonances $f_0(1200, \Gamma_0 = 100) \& f_0(1800, \Gamma_0 = 100)$.

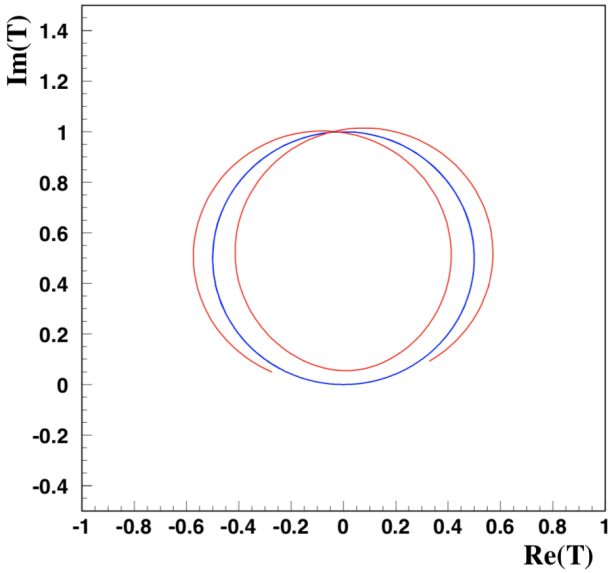

Figure 17 The Breit-Wigner model Argand diagram (red) for the case where two resonances couple to the $J^{PC} = 0^{++}$ channel with resonances $f_0(1200, \Gamma_0 = 100) \& f_0(1800, \Gamma_0 = 100)$, against a unit circle in the complex plane (unitarity not violated).

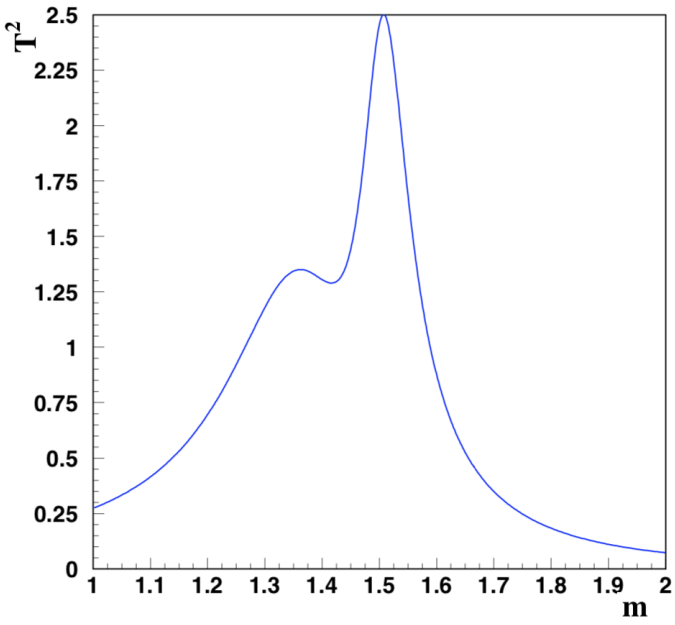

Figure 18 The Breit-Wigner model for the case where two resonances couple to the $J^{PC} = 0^{++}$ channel with resonances $f_0(1350, \Gamma_0 = 300) \& f_0(1500, \Gamma_0 = 100)$.

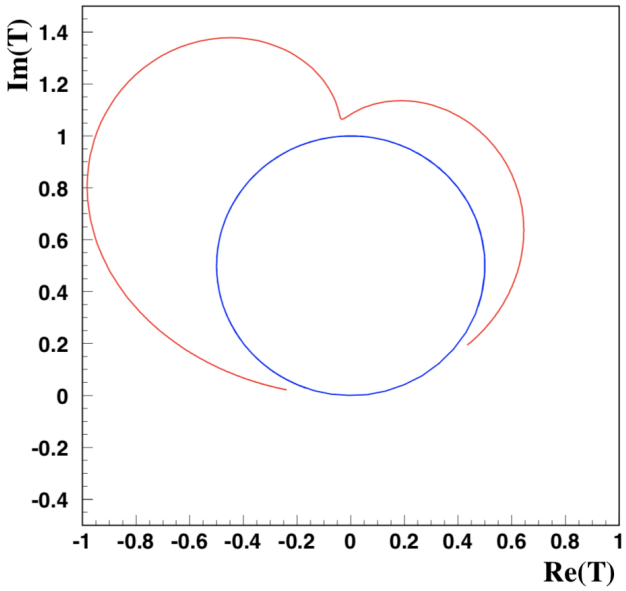

Figure 19 The Breit-Wigner model Argand diagram (red) for the case where two resonances couple to the $J^{PC} = 0^{++}$ channel with resonances $f_0(1350, \Gamma_0 = 300) \& f_0(1500, \Gamma_0 = 100)$, against a unit circle in the complex plane (unitarity not violated).

6.3 The K-Matrix formalism

The K-Matrix formalism comes out as a somewhat natural extension to the discussion in Chapter 2, where we introduced and extensively discussed, among other things, the unitarity and analyticity of the S-Matrix. Let's immediately introduce the K operator through the following expression:

$$K^{-1} = T^{-1} + iI \tag{6.15}$$

where T is the Transition operator, and we acknowledge that the K-matrix is Hermitian and may be chosen to be real and symmetric [3]. Since the K and T matrices commute, one can easily solve for T in terms of K, namely:

$$T = K(I - iK)^{-1} = (I - iK)^{-1}K \tag{6.16}$$

For a two-channel problem, we can write the K-Matrix as:

$$\begin{pmatrix} K_{11} & K_{12} \\ k_{21} & K_{22} \end{pmatrix} \tag{6.17}$$

where $K_{12} = K_{21}$, and all K_{ij} elements are real. From relation (6.16), one can obtain the following form [4]:

$$T = \frac{1}{1 - D - i(K_{11} + K_{22})} \begin{pmatrix} K_{11} - iD & K_{12} \\ K_{21} & K_{22} - iD \end{pmatrix} \tag{6.18}$$

where:

$$D = K_{11}K_{22} - K_{12}^2 \tag{6.19}$$

The transition amplitudes $\hat{T}_{ij}$, as we defined them in (3.2), are not Lorentz invariant. The Lorentz invariant transition amplitudes are given by:

$$T_{ij} = \{\rho_i\}^{1/2} \hat{T}_{ij} \{\rho_j\}^{1/2} \tag{6.20}$$

where the two-body phase space elements ρ are given by relation (6.12), where we include masses of the initial or final configuration. The invariant analog of for the K-Matrix is given by:

$$K = \{\rho\}^{1/2} \hat{K} \{\rho\}^{1/2} \tag{6.21}$$

from where we can in a fashion similar to the one for relation (6.18) obtain the following form of the invariant $\hat{T}$-Matrix, as given in Chung, S. U., Brose, J., Hackmann, R., Klempt, E., Spanier, S., & Strassburger, C. [3]:

$$\hat{T} = \frac{1}{1 - \rho_1\rho_2\hat{D} - i(\rho_1\hat{K}_{11} + \rho_2\hat{K}_{22})} \begin{pmatrix} \hat{K}_{11} - i\rho_2\hat{D} & \hat{K}_{12} \\ \hat{K}_{21} & \hat{K}_{22} - i\rho_1\hat{D} \end{pmatrix} \tag{6.22}$$

where:

$$\hat{D} = \hat{K}_{11}\hat{K}_{22} - \hat{K}_{12}^2 \tag{6.23}$$

We infer that resonances should occur as a sum of poles in the K-Matrix, where if we assume resonance domination for the amplitudes, we have:

$$K_{ij} = \sum_{\alpha} \frac{g_{\alpha i}(m) g_{\alpha j}(m)}{m_\alpha^2 - m^2} \tag{6.24}$$

or, in terms of the Lorentz invariant description [3]:

$$\hat{K}_{ij} = \sum_{\alpha} \frac{g_{\alpha i}(m) g_{\alpha j}(m)}{(m_\alpha^2 - m^2)\sqrt{\rho_i\rho_j}} \tag{6.25}$$

where the sum accounts for all the resonances α, with their respective masses m_α. The residues are given by:

$$g_{\alpha i}^2(m) = m_\alpha \Gamma_{\alpha i}(m) \tag{6.26}$$

The width $\Gamma_\alpha(m)$ is given in terms of partial widths of individual resonances as:

$$\Gamma_\alpha = \sum_i \Gamma_{\alpha i}(m) \tag{6.27}$$

where the partial widths are given as a slight reformulation of the completely analogous Eq. (6.11), namely:

$$\Gamma_{\alpha i}(m) = \gamma_{\alpha i}^2 \Gamma_\alpha^0 [B_{\alpha i}^l(q, q_\alpha)]^2 \rho_i \tag{6.28}$$

and the residues are given as:

$$g_{\alpha i}(m) = \gamma_{\alpha i} \sqrt{m_\alpha \Gamma_\alpha^0} B_{\alpha i}^l(q, q_\alpha) \sqrt{\rho_i} \tag{6.29}$$

The $B(m)$ functions are the ratios of Blatt-Weisskopf barrier factors as in (6.11), where we have labeled the brake-up momentum in channel i with q and the resonance bake-up momentum with q_α (note that the q's are equivalent to $R\rho$'s in (6.11)). Let's apply the K-Matrix formalism to the same cases as the one used for Figures 16 to 19. The K-Matrix as in (6.24) looks like [3]:

$$K_{ij}(m) = \frac{m_1 \Gamma_1(m)}{m_1^2 - m^2} + \frac{m_2 \Gamma_2(m)}{m_2^2 - m^2} \tag{6.30}$$

where the partial widths are given in Eq. (6.11). It follows from (6.22) that the T-Matrix is given by:

$$\begin{aligned} \hat{T} = & \frac{m_1 \Gamma_1(m)}{(m_1^2 - m^2) - i m_1 \Gamma_1(m) - i \dfrac{(m_1^2 - m^2)}{(m_2^2 - m^2)} m_2 \Gamma_2(m)} \\ & + \frac{m_2 \Gamma_2(m)}{(m_2^2 - m^2) - i m_2 \Gamma_2(m) - i \dfrac{(m_2^2 - m^2)}{(m_1^2 - m^2)} m_1 \Gamma_1(m)} \end{aligned} \tag{6.31}$$

We superpose the Breit-Wigner parametrization against the K-Matrix (where we plotted the $\hat{T}$-Matrix predicted intensities) in Figures 20 and 21. Clearly, there is a difference between the parameterizations, even for the case where the Breit-Wigner shouldn't be limited by any thresholds, and no significant overlap is present. More importantly, in the case where the resonances are strongly overlapping, we can

see that naive amplitude addition renders the Breit-Wigner a seriously inaccurate representation. The K-Matrix upholds the S-Matrix properties for both cases.

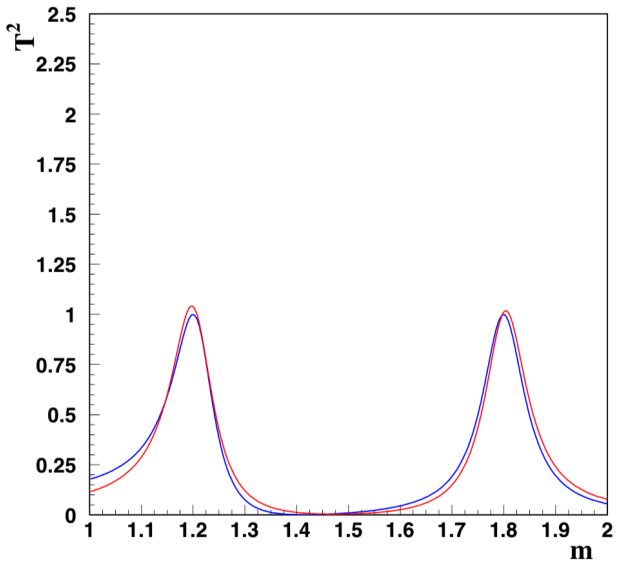

Figure 20 The Breit-Wigner model (red) and the K-Matrix (blue) model for the case where two resonances couple to the $J^{PC} = 0^{++}$ channel with resonances $f_0(1200, \Gamma_0 = 100) \& f_0(1800, \Gamma_0 = 100)$.

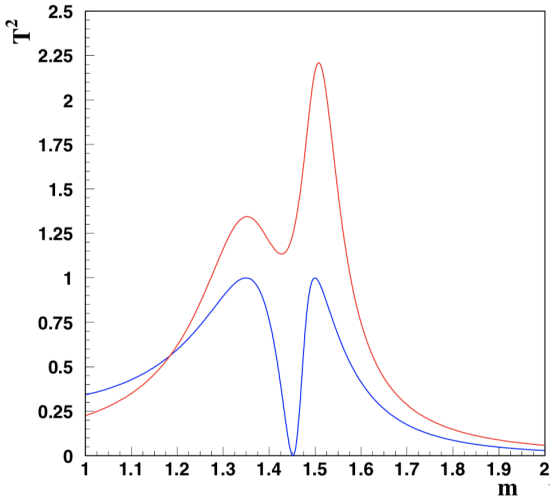

Figure 21 The Breit-Wigner model (red) and the K-Matrix (blue) model for the case where two resonances couple to the $J^{PC} = 0^{++}$ channel with resonances $f_0(1350, \Gamma_0 = 300) \& f_0(1500, \Gamma_0 = 100)$.

If the masses of the resonances are far apart, relative to their widths, the K-Matrix is dominated by a single resonance in the vicinity of its mass. In this case, it is easy to show that the formalism effectively reduces to a naive addition of Breit-Wigner's. We can see this behavior depicted in Figure 20.

There is an even larger difference, where an alternative to the Breit-Wigner is absolutely necessary. If a single resonance is coupling to several decay channels, such as is the case where a $J^{PC} = 0^{++}$ resonance such as $a_0(980)$ couples to 2 channels, $\eta\pi$ and $K\bar{K}$.

There is simply no way to represent this in terms of a Breit-Wigner, whereas a description of such cases comes naturally in the K-Matrix formalism.
Considering the case where, $a_0(980)$, a $J^{PC} = 0^{++}$ resonance, couples to 2 channels, $\eta\pi$ and $K\bar{K}$, the K-Matrix elements take the following form:

$$K_{11} = \frac{\gamma_1^2 m_0 \Gamma_0}{m_0^2 - m^2}$$
$$K_{22} = \frac{\gamma_2^2 m_0 \Gamma_0}{m_0^2 - m^2}$$
$$K_{12} = \frac{\gamma_1 \gamma_2 m_0 \Gamma_0}{m_0^2 - m^2}$$

where the T-matrix is of the following form [3]:

$$T = \frac{m_0 \Gamma_0}{m_0^2 - m^2 - i m_0 \Gamma_0 (\rho_1 \gamma_1^2 + \rho_2 \gamma_2^2)} \begin{pmatrix} \gamma_1^2 & \gamma_1\gamma_2 \\ \gamma_1\gamma_2 & \gamma_2^2 \end{pmatrix} \tag{6.32}$$

We have treated the $\gamma^{'}$s as fit parameters, where we just made sure to observe the normalization condition $\gamma_1^2 + \gamma_2^2 = 1$.

In the K-Matrix formalism, one can with a fair amount of accuracy consider individual channel contribution to the overall shape. We show this in Figures 22 to 25, where we separate the $\eta\pi$ and $K\bar{K}$ decay modes. Note that the $K\bar{K}$ contribution is scaled by a factor of hundred to be demonstrable, as the contribution is quite small compared to the $\eta\pi$. Red dots represent the resonance points.

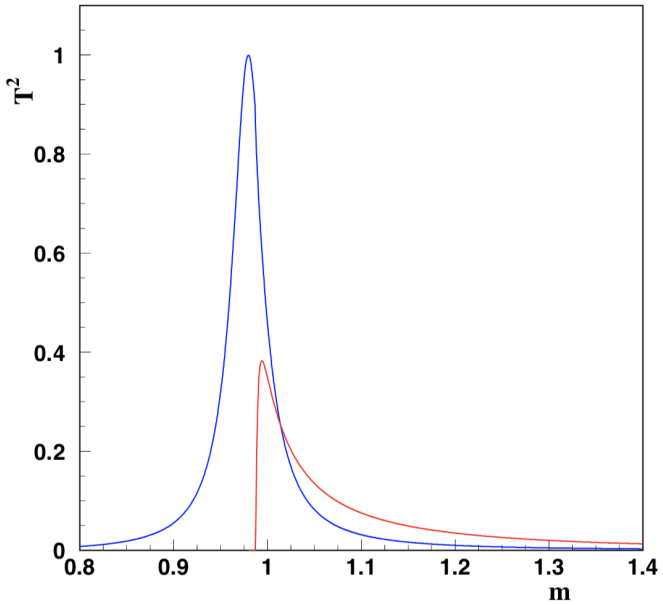

Figure 22 The $\eta\pi$ (blue) and the KK (red) channels for K-Matrix mass (0.980) and width (0.080) with $\gamma^2_{\eta\pi} = 0.8$.

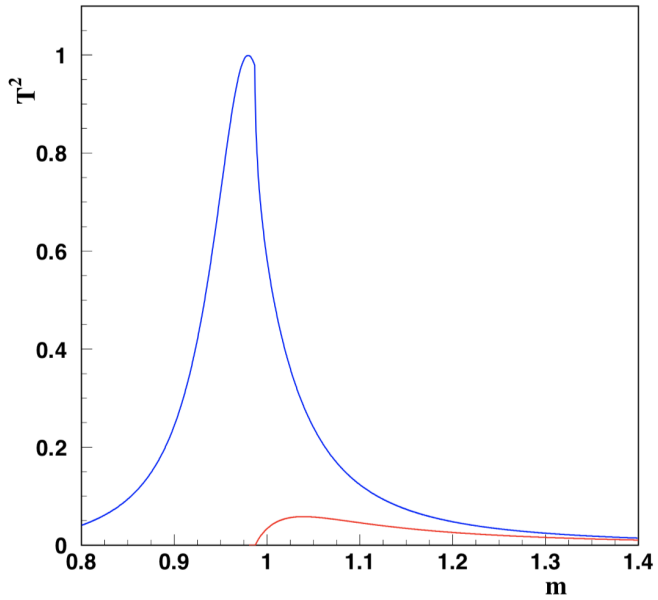

Figure 23 The $\eta\pi$ (blue) and the KK (red) channels for K-Matrix mass (0.980) and width (0.300) with $\gamma^2_{\eta\pi} = 0.5$.

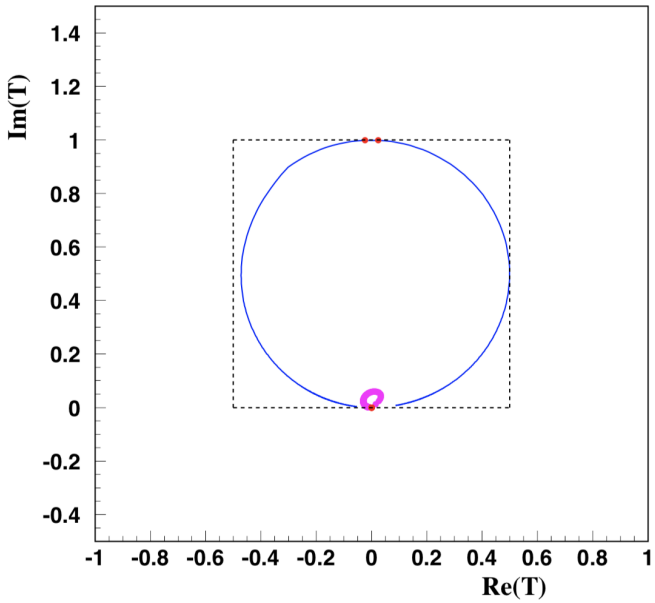

Figure 24 The Argand plots for $\eta\pi$ (blue) and the KK (red) channels for K-Matrix mass (0.980) and width (0.080) with $\gamma^2_{\eta\pi} = 0.8$.

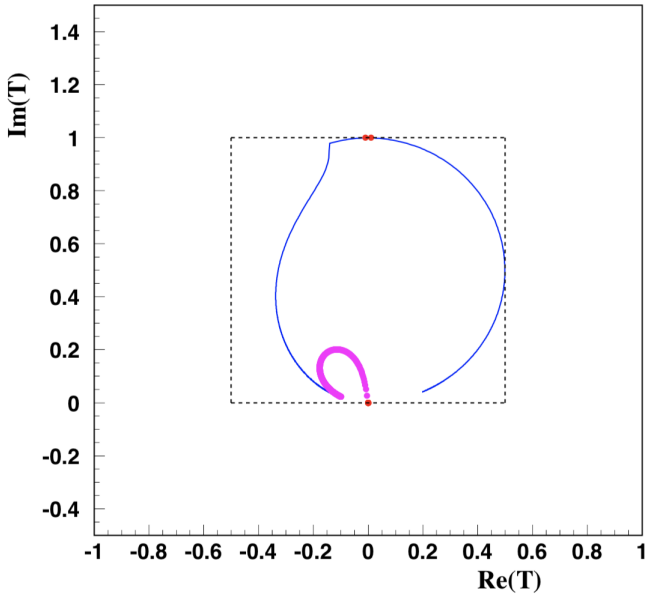

Figure 25 The Argand plots for $\eta\pi$ (blue) and the KK (red) channels for K-Matrix mass (0.980) and width (0.300) with $\gamma^2_{\eta\pi} = 0.5$.

Figures 24 and 25 demonstrate how one can gauge if such a channel contribution separation is adequate, by observing how starkly does it violate unitarity. Clearly, this is strongly dependent on the choice of $\gamma^{'}s$ and the widths of the resonances. A point must be made to the fact that it is, in fact, possible to fit a sum of Breit-Wigner's for overlapping resonances to represent the functional form quite well (especially if we leave the I wave production phases as free fit parameters). However, the masses and widths obtained from such a fit will most probably be inaccurate.

7. Partial Wave Analysis using PAWIAN (PANDA)

As previously stated, our primary motivation in this thesis was to apply PWA on exclusively centrally produced events from proton-proton collisions at ALICE. As candidate software for our purposes, we considered PAWIAN, a PWA tool made by and for the PANDA collaboration. However, at the time the thesis was being written, PAWIAN was unable to handle proton-proton collision data, and an operation mode for this purpose was in development. Therefore, we used the already functional operation mode for proton-antiproton collisions, for testing and proof of concept analysis on simulated data.

I find that is very instructive to perform such analysis, as simulating and analyzing physical data to represent a "realistic" scenario was not as trivial as it originally seemed. Points will be made in describing the main structure of PAWIAN as I find instructive. We, however, do not attempt to write a user guide. We deal with the efficiency corrections for simulated data where we didn't have the necessary MC files (detector efficiency simulation data), and finally present the analysis itself.

7.1 General PAWIAN considerations

PAWIAN has several operation modes implemented. We limit our selves to the proton-antiproton collision mode, in reference to the production mechanism of the resonance whose properties are of actual interest. There are 3 main elements one needs to consider to effectively use PAWIAN, a configuration file, a data file, and an MC file. In the configuration file, one effectively describes the process responsible for the data. Firstly, one needs to consider how to define the initial $p - \bar{p}$ system because one must provide the momentum of the system and the momentum of either the p or the $\bar{p}$. This information is necessary in order for the

program to define the quantization axes. Furthermore, the full reaction needs to be reinterpreted in terms of the isobar model, where one can define multiple two particle production instances. For the resonance of interest, one defines the decay for which one must attribute a dynamics parametrization (e.g. Breit-Wigner or K-Matrix). Finally, one must list out all the final states, in the order as given in the data file. An example configuration file can be found in Appendix B.

The analysis consists of three steps. Firstly, one needs to generate a file containing a list of the fit parameters, and initialize them. This file provides the basis for the partial wave analysis process, which produces a list of final, partial wave analysis fitted parameters. Finally, there are scripts for plotting and superimposing the data with the fitted data. This mostly means quality assurance in terms of observing and comparing angles in different frames from the data and fitted data. The cumbersome part of partial wave analysis, as hinted above, comes from our inability to deal with the number of possible fit parameters in an elegant way. One generally reverts to reducing them successively until a minimal set of partial waves is reached. PAWIAN allows for manually setting fit parameters to be constant or to exclude them completely. Here, it really comes down to whether there are some special conditions relevant to your dataset which disallow certain channels and reduce the number of fit parameters significantly. Finally, we want to have the smallest possible set of parameters which still represents the data accurately.

7.2 Efficiency Corrections for Simulated Data

As discussed in Chapter 4, for purposes of fitting to a model by means of the extended least likelihood fit, one needs an MC simulation of the detector with a flat phase space distribution of the reaction. However, since we wanted to analyze simulated data from EvtGen with PAWIAN, where it is assumed that the detector is perfectly efficient in detecting events, it is enough to provide an MC file to PAWIAN such that it can assume perfect efficiency. This means that we want a file which is an effective "spreadsheet" of isotropically distributed datapoints in mass and momentum. The requirement is that there are enough neighboring points for each data point passed to PAWIAN that the program can extrapolate the efficiency.

There are several approaches to do this, where we implemented several ourselves. An approach which allows for detail control is to start with a uniformly distributed set of mass values for a mother particle. We allow it to decay in its rest frame.

One can choose a random boost and apply it to the daughter particles. It is important to note that the direction defined by the (θ, ϕ) angles must be chosen such that it is uniformly distributed on a sphere. In term of polar coordinates, this is equivalent to generating a distribution flat in $\cos(\theta)$ and flat in ϕ. This process can be repeated as many times as necessary to represent a decay chain in terms of isobars. Note that one would need to boost the isobars with the appropriate momentum from its mother particle.

However, one must ensure that the momentum values and masses across the range are compatible one to another and properly fill the phase space. This can be quite tricky to properly implement and still maintain the flatness of the distributions. Consider a two-step decay where we are interested in a resonance X, decaying into a and b. The initial system, whose decay is leading up to the resonance formation, has to be given a range of mass values as well as boosts. These must be compatible with the masses attributed to the X and the recoil.
However, therein lies an ambiguity in how to ensure this. Naively, one might start with a random value for the mass of X in a given range. With the known mass of the recoil, one can set the possible range for the initial system mass. Therefore, we consider only the mass values of X which respect the condition that there is enough mass in the initial system to produce such a resonance-recoil pair. The non-obvious result of this selection procedure is that the mass distribution of the resonance will not be flat anymore. It is probable that this kind of a problem will pop up across all the decay chains since the flatness of mass distributions is not in any way implied by physics. The necessity of conservation laws makes maintaining flatness quite hard.

Luckily, some distributions in the MC file don't matter for us. A procedure which gives satisfying results is the reverse of the one described above. We ensure the flatness of the mass distribution (a Breit-Wigner can work as well since the mass distribution of the resonance in our dataset is a Breit-Wigner) of the resonance but not the flatness in the mass of the initial system. The momentum distribution of the initial system is ensured to be flat, and the chained decay is calculated w.r.t. the conservation laws.
The final assurance which was made is that the angular distributions of the resonance X are flat in $\cos(\theta)$ and ϕ. Note that when doing quality assurance for such a simulation, distributions should be flat in $\cos(\theta)$ and ϕ in the rest frames of their respective mother particles.

7.3 Analysis: $p\bar{p} \to f_2\pi^0 \to \pi^+\pi^-\pi^0$

This analysis was based on EvtGen simulated, chained decay, namely $p\bar{p} \to f_2\pi^0 \to \pi^+\pi^-\pi^0$. We performed the simulation in such a way that we would simulate a step of the decay chain in the rest frame of the mother and then boost the daughters. The spin density matrix for the $p\bar{p}$ system decay was set to a normalized diagonal 3×3 matrix. The $f_2(1270)$ decay spin density matrix was made such that the only surviving contribution was from the D^2_{00} D-Wigner function (see Eq. (5.34)). Example code for data simulation using EvtGen is shown in Appendix A. The base information going in to the analysis were that the $p\bar{p}$ is a $I^G(J^{PC}) = 1^-(0^{+-})$ state, while, as previously stated, the $f_2(1270)$ is a $I^G(J^{PC}) = 0^+(2^{++})$ state. The two pions are $I^G(J^{PC}) = 1^-(0^+)$ states. In order to truncate the set of possible amplitudes coming from the production mechanism, and have a direct link with the theoretically predicted distributions, we limited the angular momentum between the recoil pion and the $f_2(1270)$ to $L = 2$.

Having in mind that $\lambda = \lambda_1 - \lambda_2$, $J_{p\bar{p}} = 0$ and $J_{f_2\pi^0} = 2$, the full amplitude is given by [4]:

$$A^{JM}_{\lambda_1\lambda_2}(\Omega_1, \Omega_2) = A^{00}_{00}(\Omega_{f_2\pi^0}) A^{00}_{20}(\Omega_{\pi^+\pi^-}) \tag{7.1}$$

where we note that the $A^{00}_{00}(\Omega_{f_2\pi^0})$ amplitude is really just a scaling constant (the D^0_{00} D-Wigner function is equal to unity).

Note that while simulating the data there is a subtlety that came up when we ran the EvtGen simulated data trough PAWIAN. The plots of pure data didn't correspond one to another when plotted directly from EvtGen and trough PAWIAN. One must take care when simulating decays of a resonance which is not at rest. Even though EvtGen always simulates decays in the rest frame of the mother particle, when traversing from the Lab frame to the Helicity frame and vice versa, it becomes important whether one rotates the reference system and then boosts it, or the does the reverse. This is purely due to the fact that the program cannot work in terms of abstract notions of relative coordinate systems, even though the concept is perfectly clear. Theoretically, the procedure remains insensitive to the order of operations.

The MC data was simulated such that the $p\bar{p}$ system had a flat distribution in momentum, while the $f_2(1270)$ was simulated such that it had a flat distribution in mass, $\cos(\theta)$ and ϕ. Example code for such a simulation is provided in Appendix C. The relevant distributions are shown in Figures 26 to 30.

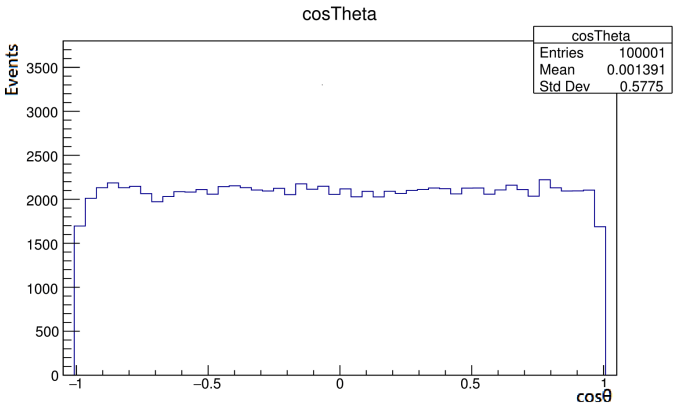

Figure 26 The MC data distribution in $\cos(\theta)$ for $f_2(1270)$ w.r.t the $p\bar{p}$ system (restframe).

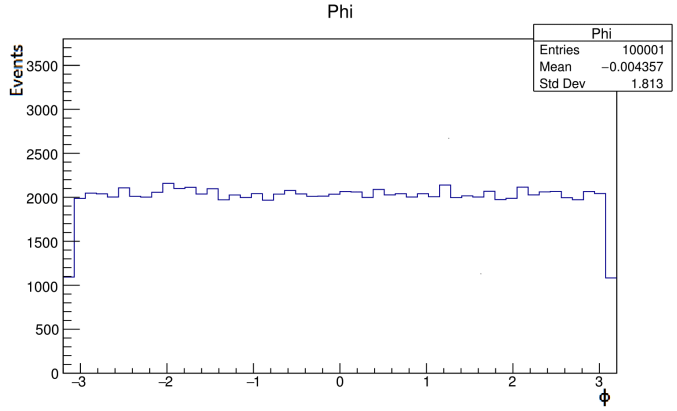

Figure 27 The MC data distribution in ϕ for $f_2(1270)$ w.r.t the $p\bar{p}$ system (restframe).

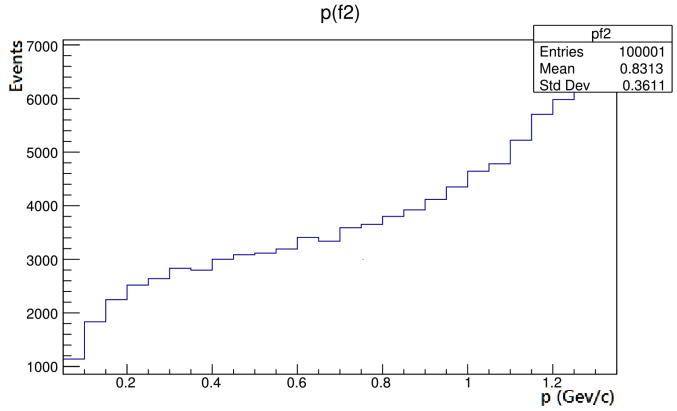

Figure 28 The MC data distribution in mass for $f_2(1270)$.

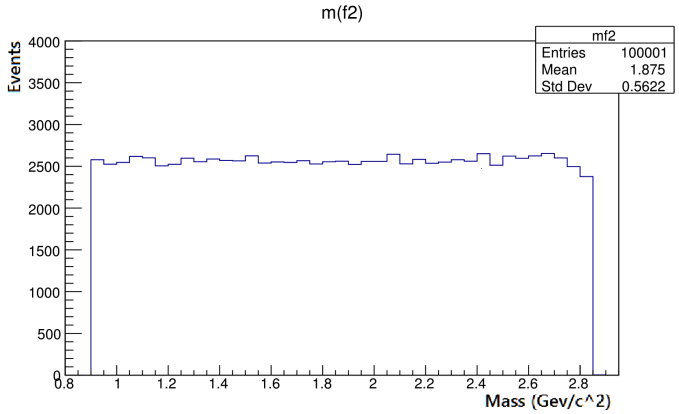

Figure 29 The MC data distribution in momentum magnitude for $f_2(1270)$.

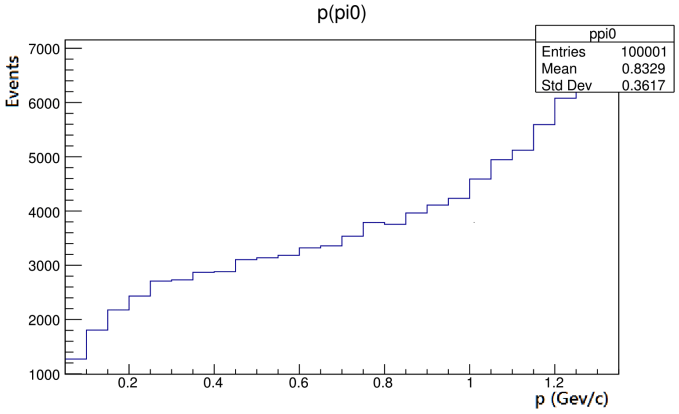

Figure 30 The MC data distribution in momentum magnitude for π^0. Note that π^0 had a fixed mass in our MC Simulations.

In PAWIAN, we excluded all of the initial fit parameters except the ones contained in the only two possible amplitudes that respect our assumptions. For quality assurance, we superposed the PAWIAN calculated distributions against the data for the $\cos(\theta)$ and ϕ distributions of the π^+ w.r.t the $f_2(1270)$ in both the Helicity and the Gottfried-Jackson frame [23], along with a customary mass fit for the $f_2(1270)$. The results of the analysis are shown in Figures 31 to 35.

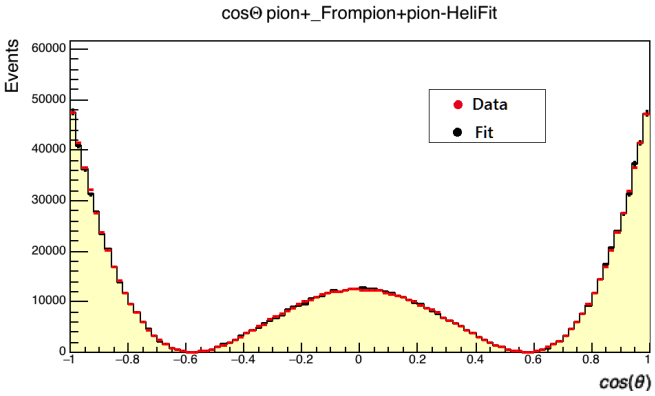

Figure 31 The quality assurance for the $\cos(\theta)$ distribution for π^+ w.r.t $f_2(1270)$ in the Helicity frame.

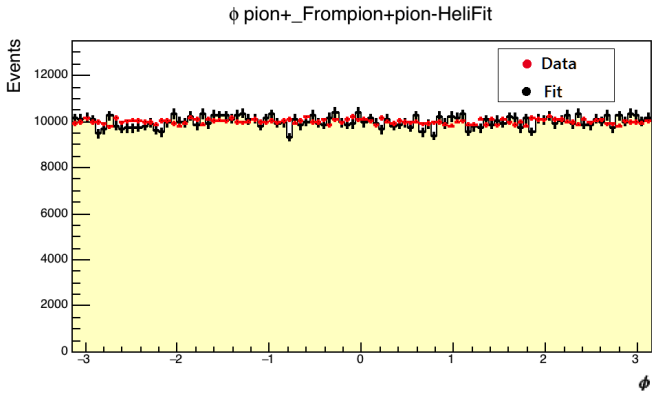

Figure 32 The quality assurance for the ϕ distribution for π^+ w.r.t $f_2(1270)$ in the Helicity frame.

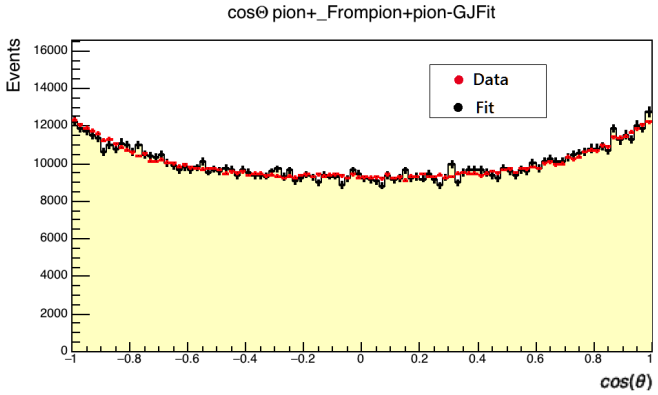

Figure 33 The quality assurance for the $\cos(\theta)$ distribution for π^+ w.r.t $f_2(1270)$ in the Gottfried-Jackson frame.

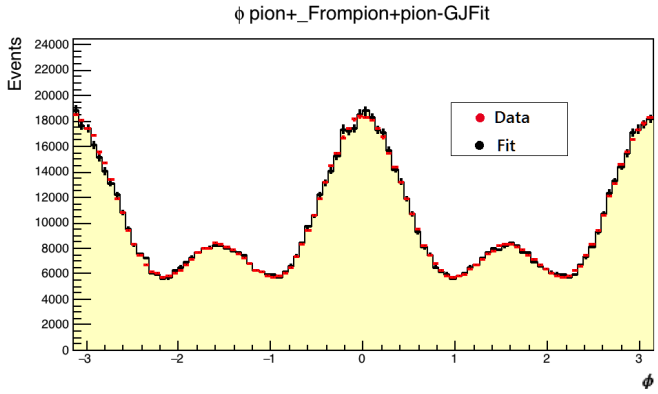

Figure 34 The quality assurance for the ϕ distribution for π^+ w.r.t $f_2(1270)$ in the Gottfried-Jackson frame.

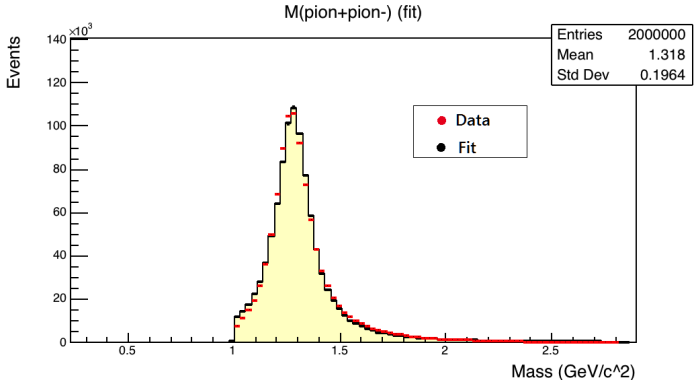

Figure 35 The mass fit for $f_2(1270)$ from PAWIAN.

As we can see, the fit seems to represent the data well, with the mass fit reproducing the expected mass closely. Note that the distribution in $\cos(\theta)$ shown in Figure 31, corresponds to the θ distribution shown in Figure 10. This is not the only combination of the amplitudes which would reproduce the same angular distributions and mass. Surely the more fit parameters are present and left free, the more "probable" would it be to find a matching. The resulting fit parameters from the analysis with the truncated set of amplitudes and for the full set of non-fixed amplitudes are shown in Appendix D. However, this certainly is the minimal set of amplitudes which can be fitted faithfully. Obviously, this was an educated guess since we simulated the data in a controlled way with strong theoretical foundation and motivation.

In general, one cannot make such predictions and conclusion a priori. Furthermore, the intermediate resonant formation and its nature can in general only be speculated from the invariant mass spectrum, which will almost certainly contain several resonances, quite possibly overlapping ones, with several coupled decay channels. This makes for a lot of bad assumptions, and trial and error, and usually results in several ambiguous "solutions", which it might be difficult to discriminate.
As a final remark, we want to stress that one should take care that the MC file and the data file cover the same range. If the MC data didn't contain i.e. masses lower than one, but the data file did, the fit would not be performed against the entire dataset. Notice that in Figures 31 to 35, the data and the MC file don't contain $f_2(1270)$ mass values lower than one. This was the default setting in EvtGen when simulating the $f_2(1270)$ resonance and we choose to use it.
We don't include the mass fit for the MC file, where we generated the mass of the $f_2(1270)$ from the flat distribution in $p\bar{p}$ mass, by means of conservation laws. The bias in the mass fit is present, but hard to notice. The effects of on non-flat distributions in $cos\theta$ and ϕ in the MC file caused the fitting procedure to fail completely, and hence cannot be demonstrated here.

8. Conclusion

It would have been quite a precedent to have managed to present conclusions from the first pp collision CEP data analysis on behalf of the ALICE collaboration. We have however not managed to come quite so far. The time stipulated for the research and the writing of the thesis made this out of our reach. It remains that we have tested out, implemented and gained experience in PWA. We delved with the key concepts of Regge theory, and as such feel confident in drawing a conclusion from any further research on this filed. This knowledge is hopefully adequately presented in the thesis and should allow fellow physicists to continue the research without having to invest the time we had to in understanding the base constituents.

Rather than to conclude on an apologetic note, it might be more useful to outline the basic idea and approach in implementing the pp collision mode into PAWIAN, we have been working on with the PANDA collaboration. In order to make sense of this, we must present a set of experimental limitations we have with the ALICE detector, which largely steered us towards the current attempt at implementation.

Outside the rather obvious limitation imposed by our inability to detect uncharged particles, the main complication arises due to not measuring the final states of the pp system. Together with an unpolarized beam for the initial pp system, this makes it impossible to define a CEP process in terms of isobars, as described by the data gathered by the ALICE detector. An unpolarized beam leaves no room for manipulating the fit with the spin density matrix. There, the only possibility of obtaining non-trivial angular distributions would arise due to a coupled chain of decays. However, we don't measure the data necessary to fit the amplitudes for the production mechanism. Perhaps these points are more transparent if presented in context, for example, if we are trying to analyze the following reaction: $pp \to pp f_2(1270) \to pp\pi^+\pi^-$.

One says the pp system and the proposition of the production mechanism (currently considering only the DPE mechanism) define the possible initial quantum states, which in term, together with a hypothesis for the final states defines the possible helicity states of the resonance we are investigating (in this example we are insinuating the resonance in question if the $f_2(1270)$, perhaps from the invariant mass spectrum).One sais the pp system and the production mechanism (currently considering only the DPE mechanism) define the possible initial quantum states.

Together with a hypothesis for the final states, this defines the possible helicity states of the resonance we are investigating (in this example we are insinuating the resonance in question if the $f_2(1270)$, perhaps from the invariant mass spectrum). This actually allows us to reinterpret the production amplitudes. Contextually, it is equivalent to, rather than defining a production amplitude in terms of the actual decay, taking the amplitude for the $f_2(1270)$ to have some helicity value. Since we know the J and λ, we can define the D-Wigner constituents. The corresponding production fit parameters can be taken to be functionally analog to the amplitudes defined for the decay. As proposed by our colleagues in the PANDA collaboration, we can write the cross-section to be proportional to an incoherent summation over the helicities of the resonance and the final state particles, given by the following relation:

$$\frac{d\sigma}{d\tau} \propto \sum_{\lambda_x=-J_x}^{+J_x} \sum_{\lambda_{FS}} |\sqrt{\frac{2J_x+1}{4\pi}} F_{\lambda_a,\lambda_b} D^{J_x*}_{\lambda_x,\lambda_a-\lambda_b}(\phi,\theta) \bar{F_{L_x}}(m_x)|^2 \qquad (8.1)$$

where the the complex helicity amplitude F_{λ_a,λ_b} and the energy-dependent part of the amplitude $\bar{F_{L_x}}(m_x)$ are fit parameters. The $D^{J_x*}_{\lambda_x,\lambda_a-\lambda_b}(\phi,\theta)$ denotes the aforementioned D-Wigner functions.

A proper implementation of a pp collision mode into PAWAIN may prove a useful tool in the analysis of pp collision CEP data. I hope this thesis may prove useful to anyone interested in this phenomenology, and enable a more seamless introduction to the problem at hand.

9. Appendix A

The code below will produce data as described in Chapter 7, using $EvtGen$. There is additional functionality, as an inspection of the code will reveal. Extensive use of $EvtGen$ as well as $ROOT$ implemented classes has been made, in addition to the general environment of $C++$. The output of the macro is formatted such that is can be directly used by $PAWIAN$. To help to understand the code, there are short comments scattered throughout. For clarification of EvtGen specific classes, as well as the general EvtGen framework questions, refer to Lange, D. J. [18]. For ROOT specific classes refer to Brun, R., & Rademakers, F. [24].

```
#include "EvtGenBase/EvtComplex.hh"
#include "EvtGenBase/EvtTensor4C.hh"
#include "EvtGenBase/EvtVector4C.hh"
#include "EvtGenBase/EvtVector4R.hh"
#include "EvtGenBase/EvtVectorParticle.hh"
#include "EvtGenBase/EvtDiracSpinor.hh"
#include "EvtGenBase/EvtParticle.hh"
#include "EvtGenBase/EvtKine.hh"
#include "EvtGenBase/EvtGammaMatrix.hh"
#include "EvtGenBase/EvtRandom.hh"
#include "EvtGenBase/EvtRandomEngine.hh"
#include "EvtGenBase/EvtDecayTable.hh"
#include "EvtGenBase/EvtReport.hh"
#include "EvtGenBase/EvtPDL.hh"
#include "EvtGenBase/EvtStdHep.hh"
#include "EvtGenBase/EvtSecondary.hh"
#include "EvtGenBase/EvtConst.hh"
#include "EvtGen/EvtGen.hh"
#include "EvtGenBase/EvtParticleFactory.hh"
#include "EvtGenBase/EvtSimpleRandomEngine.hh"
#include "EvtGenBase/EvtMTRandomEngine.hh"
#include "EvtGenBase/EvtIdSet.hh"
#include "EvtGenBase/EvtParser.hh"
#include "EvtGenBase/EvtAbsRadCorr.hh"
#include "EvtGenBase/EvtDecayBase.hh"
#ifdef EVTGEN_EXTERNAL
#include "EvtGenExternal/EvtExternalGenList.hh"
#endif
#include <cstdio>
#include <fstream>
#include <sstream>
```

```
#include <cmath>
#include <string>
#include <vector>
#include <cstdlib>
#include "TClonesArray.h"
#include "TH1.h"
#include "TH2.h"
#include "TTree.h"
#include "TFile.h"
#include "TApplication.h"
#include "TROOT.h"
#include <stdlib.h>
#include <TList.h>
#include <TLorentzVector.h>
#include <TH1D.h>
#include <TF1.h>
#include <vector>
#include "TCanvas.h"
#include <cmath>
#include <TH2D.h>
#include <cstring>
#include <functional>
#include <iostream>

using std::vector;
const double pi = 3.14159265358;
void runHelAmp(int nevent, EvtGen & myGenerator, std::string userFile,
               std::string rootFile);

int main(int argc, char *argv[])
{

  // Define the random number generator
  EvtRandomEngine *myRandomEngine = 0;

#ifdef EVTGEN_CPP11
  // Use the Mersenne-Twister generator (C++11 only)
  myRandomEngine = new EvtMTRandomEngine();
#else
  myRandomEngine = new EvtSimpleRandomEngine();
#endif

  if (!TROOT::Initialized()) {
    static TROOT root("RooTuple", "RooTuple ROOT in EvtGen");
  }

  EvtAbsRadCorr *radCorrEngine = 0;
  std::list < EvtDecayBase * >extraModels;
```

```
#ifdef EVTGEN_EXTERNAL
  EvtExternalGenList genList;
  radCorrEngine = genList.getPhotosModel();
  extraModels = genList.getListOfModels();
#endif
  std::string mystring =
      std::string(getenv("EVTGEN_BASE")) + std::string("/DECAY_2010.DEC");
  std::string yourstring =
      std::string(getenv("EVTGEN_BASE")) + std::string("/evt.pdl");
  EvtGen myGenerator(mystring.c_str(), yourstring.c_str(), myRandomEngine,
                     radCorrEngine, &extraModels);
  int nevent = atoi(argv[1]);
  runHelAmp(nevent, myGenerator, "HELYTEST1.DEC", "results/f_2.root");

}

void runHelAmp (
  int nevent,
  EvtGen & myGenerator,
  std::string userFile,
  std::string rootFile )
{

  // get decay information from HELYTEST1.DEC
  myGenerator.readUDecay(userFile.c_str());

        // result root file
  TFile *file = new TFile(rootFile.c_str(), "RECREATE");
  TTree *tree = new TTree("hidden treasure", "to be explored");
  Int_t evn = 0;
  Int_t pdg = 0;
  Double_t prza = 0;
  Double_t px = 0;
  Double_t py = 0;
  Double_t pz = 0;

  tree->Branch("EVN", &evn);
  tree->Branch("PDG", &pdg);
  tree->Branch("E", &prza);
  tree->Branch("px", &px);
  tree->Branch("py", &py);
  tree->Branch("pz", &pz);

  // open output file for 4-vectors which is used as input for PAWIAN
  FILE *fftxt = fopen ("results/Evtgen_to_pipipi.dat","w");
  // initialize he random generator
  EvtRandomEngine *rndgen = new EvtSimpleRandomEngine();
  // some definitions
  static EvtId pBp = EvtPDL::getId(std::string("pbarpSystem"));
```

```
EvtParticle *f2tag = NULL;
EvtParticle *pi0 = NULL;
EvtParticle *pic[2] = {NULL};
EvtVector4R lv;
Double_t ptot, norm;
Double_t mass, ene;
EvtVector4R vf2;
TVector3 az = TVector3(0,0,1),rota,bv;
TLorentzVector lvf2,lvtmp,lvHel;
Double_t ang;

// event counter
// counter[0]: number of generated events
// counter[1]: number of pbarp -> f2 + pi0
// counter[2]: number of pbarp -> pi+ + pi- + pi0
Int_t counter[3] = {0};
do {
  // create pbarp system
  // select random momentum
  px = rndgen->random();
  py = rndgen->random();
  pz = rndgen->random();
  ptot = sqrt(px * px + py * py + pz * pz);
  norm = 3 * rndgen->random();
  px = px / ptot * norm;
  py = py / ptot * norm;
  pz = pz / ptot * norm;
  // the initial pbarpSystem is defined in evt.pdl
  // currently it has a mass of 2.98 GeV/c^2, the mass of eta_c
  mass = EvtPDL::getMass(pBp);
  ene = sqrt(mass * mass + px * px + py * py + pz * pz);
  // but then intialize it with p=0
  // ATTENTION: this is useless if results are not boosted later on
  EvtVector4R p_init(EvtPDL::getMass(pBp), 0.0, 0.0, 0.0);
  EvtParticle *root_part = EvtParticleFactory::particleFactory(pBp,p_init);
  // define density matrix of initial system
  EvtSpinDensity rho;
  rho.setDiag(3);
  // let the initial system decay - it decays at rest !!
  EvtGenReport(EVTGEN_ERROR,"notevtgen") <<
                      root_part->getSpinDensityForward();
  myGenerator.generateDecay(root_part);

  if (!(counter[0] % 10000)) printf("event %4.4i\n", counter[0]);

  // select events ppbar -> f2 + pi0
  // f2tag: f2
  // pi0:   pi0
  f2tag = NULL; pi0   = NULL;
```

```
if (root_part->getNDaug()==2) {
  for (Int_t ii = 0; ii < root_part->getNDaug(); ii++) {
    if (root_part->getDaug(ii)->getPDGId()==225)
      f2tag=root_part->getDaug(ii);
    if (root_part->getDaug(ii)->getPDGId()==111)
      pi0=root_part->getDaug(ii);
  }
}
if (f2tag && pi0) {
  counter[1]++;
  // prepare for transformation to helicity frame
  vf2  = f2tag->getP4Lab();
  lvf2 = TLorentzVector(vf2.get(1),vf2.get(2),vf2.get(3),vf2.get(0));
  rota = lvf2.Vect().Cross(az);
  ang  = lvf2.Vect().Angle(az);
  lvf2.Rotate(ang,rota);
  bv   = lvf2.BoostVector();

  // set momentum of f2 to 0
  // let f2 decay at rest to get the proper angular distributions
  // then boost the daughter particles along z
  // and finally rotate the daughters
  EvtId id = f2tag->getId();
  EvtVector4R a = f2tag->getP4Restframe();
  f2tag->init(id,a);

  // set density matrix of f2
  EvtSpinDensity rishloo;
  rishloo.setDiag(5);
  rishloo.set(0, 0, EvtComplex(0.0, 0.0));
  rishloo.set(1, 1, EvtComplex(0.0, 0.0));
  rishloo.set(2, 2, EvtComplex(1.0, 0.0));
  rishloo.set(3, 3, EvtComplex(0.0, 0.0));
  rishloo.set(4, 4, EvtComplex(0.0, 0.0));
  f2tag->setSpinDensityForwardHelicityBasis(rishloo);

  // let f2 decay
  myGenerator.generateDecay(f2tag);

  // select f2 -> pi+ + pi-
  // pic[0]: pi-
  // pic[1]: pi+
  pic[0] = NULL; pic[1] = NULL;
  if (f2tag->getNDaug()==2) {
    for (Int_t ii = 0; ii < f2tag->getNDaug(); ii++) {
      if (f2tag->getDaug(ii)->getPDGId()==-211)
        pic[0]=f2tag->getDaug(ii);
      if (f2tag->getDaug(ii)->getPDGId()==211)
        pic[1]=f2tag->getDaug(ii);
```

```
    }
  }

  if (pic[0] && pic[1]) {
    counter[2]++;
    // increment book keeper
    evn++;

    // fill 3 pions - pi-, pi+, pi0
    for (Int_t ii=0; ii<3; ii++) {
      if (ii<2) {
        lv = pic[ii]->getP4Lab();

        // boost pi- along z and rotate to be in the lab-frame
        lvtmp = TLorentzVector(lv.get(1),lv.get(2),lv.get(3),lv.get(0));
        lvtmp.Boost(bv);
        lvtmp.Rotate(-ang,rota);

        if (ii == 0) {
          // transform pi- into Helicity frame
          lvHel = lvtmp;
          lvHel.Rotate(ang,rota);
          lvHel.Boost(-bv);
          double c = lvHel.CosTheta();
          double d = lvHel.Phi();
          pdg = -211;
        } else {
          pdg = 211;
        }
      }
      else {
        lv = pi0->getP4Lab();
        lvtmp = TLorentzVector(lv.get(1),lv.get(2),lv.get(3),lv.get(0));
        pdg = 111;
      }
      // update txt file
      fprintf(fftxt,"%11.8f %11.8f %11.8f %11.8f\n",
        lvtmp.E(),
        lvtmp.X(),
        lvtmp.Y(),
        lvtmp.Z()
      );
      // fill tree
      prza = lvtmp.E();
      px = lvtmp.X();
      py = lvtmp.Y();
      pz = lvtmp.Z();
      tree->Fill();
    }
```

```
      }
    }
    root_part->deleteTree();
  } while (counter[0]++ < nevent);
  printf("events: %i %i %i\n",counter[0],counter[1],counter[2]);
  file->Write();
  file->Close();
  fclose(fftxt);
  EvtGenReport(EVTGEN_INFO, "EvtGen") << "SUCCESS\n";
}

#
#
#
noPhotos
#
Decay pbarpSystem
 1.0   f_2   pi0                                          PHSP;
Enddecay
#
Decay f_2
1.0000   pi+  pi-                                        HELAMP 1.0 0.0;
Enddecay
#
Decay pi0
0.988228297 gamma   gamma                                 PHSP;
0.011738247 e+      e-      gamma                         PI0_DALITZ;
0.000033392 e+      e+      e-      e-                    PHSP;
0.000000065 e+      e-                                    PHSP;
Enddecay
#
Decay K_L0
#0.202464226 pi+     e-      nu_e                          PHSP;
#0.202464226 pi-     e+      nu_e                          PHSP;
#0.135033299 pi+     mu-     nu_mu                         PHSP;
#0.135033299 pi-     mu+     nu_mu                         PHSP;
#0.000025738 pi0     pi+     e-      nu_e                  PHSP;
#0.000025738 pi0     pi-     e+      nu_e                  PHSP;
#0.000006205 pi+     e-      nu_e    e+      e-            PHSP;
#0.000006205 pi-     e+      nu_e    e+      e-            PHSP;
#0.194795855 pi0     pi0     pi0                           PHSP;
#0.125231606 pi+     pi-     pi0                           PHSP;
#0.001880711 pi+     e-      nu_e    gamma                 PHSP;
#0.001880711 pi-     e+      nu_e    gamma                 PHSP;
#0.000277023 pi+     mu-     nu_mu   gamma                 PHSP;
#0.000277023 pi-     mu+     nu_mu   gamma                 PHSP;
#0.000040995 pi+     pi-     gamma                         PHSP;
#0.000001262 pi0     gamma   gamma                         PHSP;
#0.000000016 pi0     gamma   e+      e-                    PHSP;
```

```
#0.000545653  gamma    gamma                                    PHSP;
#0.000009265  e+       e-       gamma                           PHSP;
#0.000000355  mu+      mu-      gamma                           PHSP;
#0.000000584  e+       e-       gamma     gamma                 PHSP;
#0.000000007  mu+      mu-      gamma     gamma                 PHSP;
Enddecay
#
Decay K_S0
0.691321852  pi+      pi-                                      PHSP;
0.306221852  pi0      pi0                                      PHSP;
0.000000201  pi+      pi-      pi0                             PHSP;
0.001722185  pi+      pi-      gamma                           PHSP;
0.000042831  pi+      pi-      e+        e-                    PHSP;
0.000000025  pi0      gamma    gamma                           PHSP;
0.000002399  gamma    gamma                                    PHSP;
0.000344328  pi+      e-       nu_e                            PHSP;
0.000344328  pi-      e+       nu_e                            PHSP;
Enddecay
#
Decay eta
0.393100000  gamma    gamma                                    PHSP;
0.325700000  pi0      pi0      pi0                             PHSP;
0.227400000  pi-      pi+      pi0                             ETA_DALITZ;
0.046000000  gamma    pi-      pi+                             PHSP;
0.007000000  gamma    e+       e-                              PHSP;
0.000310000  gamma    mu+      mu-                             PHSP;
0.000214200  pi+      pi-      e+        e-                    PHSP;
0.000005800  mu+      mu-                                      PHSP;
Enddecay
#
End
```

10. Appendix B

This configuration file for PAWIAN should, if used with properly simulated data (Appendix A) and proper MC data (Appendix C), reproduce the fit parameters resulting in Figures 31 to 35 (Chapter 7). Note that in this example code, we fix many fit parameters. This should go in conjunction with parameter initializations such that all amplitudes which are set fixed should be fixed to value 0. This will result in a fit using the minimal set of amplitudes which describes the data. For more detail on the structure, further options in the configuration file and general PAWIAN related questions refer to PAWIAN website.

```
errLogMode = trace
```

```
datFile     = ./Evtgen_to_pipipi.dat
mcFile      = ./iso_to_pipipi.dat
unitInFile = GEV
orderInFile = E Px Py Pz
paramFile = ./defaultparams_f_2.dat
name = _f_2

ratioMcToData  = 10
initial4Vec = 2.98 0 0 0
projectile4Vec = 9.3827205e-01 0 0 1.0
useDataEventWeight = true
useMCEventWeight = false
mode = pwa
verbose = 1

finalStateParticle = pion-
finalStateParticle = pion+
finalStateParticle = pion0

fitqRProduction = false
usePhaseSpaceHyp = false

# Productions
production = f2(1270) pion0

# Decays
decay = Cano noIso f2(1270) To pion+ pion-

#Dynamics
addDynamics = f2(1270) BreitWignerBlattWRel

#Histogramms
histMass = pion+ pion-
histAngles = pion+ from pion+ pion-

#Fixed Parameter
# Masses, widths
mnParFix = L1S2_J1P1C1Tof2(1270)_pion0Mag
mnParFix = L1S2_J1P1C1Tof2(1270)_pion0Phi
mnParFix = L3S2_J1P1C1Tof2(1270)_pion0Mag
mnParFix = L3S2_J1P1C1Tof2(1270)_pion0Phi
mnParFix = L0S2_J2P-1C1Tof2(1270)_pion0Mag
mnParFix = L0S2_J2P-1C1Tof2(1270)_pion0Phi
mnParFix = L2S2_J2P-1C1Tof2(1270)_pion0Mag
mnParFix = L2S2_J2P-1C1Tof2(1270)_pion0Phi
mnParFix = L4S2_J2P-1C1Tof2(1270)_pion0Mag
mnParFix = L4S2_J2P-1C1Tof2(1270)_pion0Phi
mnParFix = L1S2_J2P1C1Tof2(1270)_pion0Mag
mnParFix = L1S2_J2P1C1Tof2(1270)_pion0Phi
```

```
mnParFix = L3S2_J2P1C1Tof2(1270)_pion0Mag
mnParFix = L3S2_J2P1C1Tof2(1270)_pion0Phi
mnParFix = L1S2_J3P1C1Tof2(1270)_pion0Mag
mnParFix = L1S2_J3P1C1Tof2(1270)_pion0Phi
mnParFix = L3S2_J3P1C1Tof2(1270)_pion0Mag
mnParFix = L3S2_J3P1C1Tof2(1270)_pion0Phi
mnParFix = L5S2_J3P1C1Tof2(1270)_pion0Mag
mnParFix = L5S2_J3P1C1Tof2(1270)_pion0Phi
mnParFix = L3S2_J4P1C1Tof2(1270)_pion0Mag
mnParFix = L3S2_J4P1C1Tof2(1270)_pion0Phi
mnParFix = L5S2_J4P1C1Tof2(1270)_pion0Mag
mnParFix = L5S2_J4P1C1Tof2(1270)_pion0Phi
#mnParFix = f2(1270)Mass
#mnParFix = f2(1270)Width

pdgTableFile = /Particle/pdtNew.table
cacheAmps = true
serverPort = 50001
serverAddress = localhost
noOfClients = 2
noOfThreads = 18
evoIterations = 50
evoPopulation = 160
evoRatioOfModParams = 0.05
```

11. Appendix C

Here, we provide an example code which will generate distributions flat in the mass of the $f_2(1270)$, and flat in $cos\theta$ and ϕ (described in Chapter 7). Note that this macro is made so there are a plethora of histograms for all o the relevant quantities, without which it would be rather hard to be certain we actually produce what we wanted to produce. The output of the macro is formatted to directly be used by PAWIAN. In an attempt to help to understand the code, there are short comments scattered throughout. For ROOT specific classes refer to Brun, R., & Rademakers, F. [24].

```
#include <stdio.h>

#include "TVector3.h"
#include "TMath.h"
#include "TRandom.h"
#include "TLorentzVector.h"
#include "TFile.h"
```

```
#include "TTree.h"
#include "TH1F.h"

// unit of mass in Mev/c^2
static const double pi2 = 2.*3.1415926;
static const double Einimin  = 2.980;
static const double Einimax  = 2.986;
static const double ptotmin  = 0.0;
static const double ptotmax  = 0.1;
static const double mf2min   = 0.9;
static const double mf2max   = 3.0;
static const double mpi0min  = 0.1349760;
static const double mpi0max  = 0.1349772;
static const double mpimin   = 0.13957055;
static const double mpimax   = 0.13957066;
static const double mpi1     = 0.13957061;
static const double mpi2     = 0.13957061;

int main(int argc, char *argv[])
{

  // 1st argument is number of events
  // 2nd argument is the name of the signal file
  // 3d argument is a version string
  Int_t np = atoi(argv[1]);
  TString sigfn = TString(argv[2]);
  TString version = TString(argv[3]);

  // some initialisations
  Double_t theta, phi;

  // 5 particles are involved
  // ini, f2, pi0, pi1 (=pi-), pi2 (=pi+)
  Double_t        Eini, Ef2, Epi0, Epi1, Epi2;
  Double_t        pini, pf2, ppi1;
  Double_t        mini, mf2, mpi0, mpi1, mpi2;
  TVector3        pvini, pvf2, pvpi0, pvpi1, pvpi2;
  TLorentzVector lvini, lvf2, lvpi0, lvpi1, lvpi2;

  // random generator
  TRandom rnd = TRandom(0);

  // open output file for histograms
  TString rootfn = Form("results/iso_to_pipipi_%s.root",version.Data());
  TFile *ffroot = new TFile(rootfn.Data(),"RECREATE");

  // histograms for all particles
  // pbarp system properties
  TH1F *hEini  = new TH1F("Eini","Eini",100,Einimin-0.01,Einimax+0.01);
```

```
TH1F *hmini  = new TH1F("mini","mini",100,Einimin-0.02,Einimax);
TH1F *hpini  = new TH1F("pini","pini",100,-0.1,ptotmax+0.1);
TH1F *hpxini = new TH1F("pxini","pxini",100,-ptotmax,ptotmax);
TH1F *hpyini = new TH1F("pyini","pyini",100,-ptotmax,ptotmax);
TH1F *hpzini = new TH1F("pzini","pzini",100,-ptotmax,ptotmax);

// f2 properties
TH1F *hEf2  = new TH1F("Ef2","Ef2",100,mf2min,mf2max+0.5);
TH1F *hmf2  = new TH1F("mf2","mf2",100,mf2min,mf2max);
TH1F *hpf2  = new TH1F("pf2","pf2",100,-0.1,2.0);
TH1F *hpxf2 = new TH1F("pxf2","pxf2",100,-1.5,1.5);
TH1F *hpyf2 = new TH1F("pyf2","pyf2",100,-1.5,1.5);
TH1F *hpzf2 = new TH1F("pzf2","pzf2",100,-1.5,1.5);

// pi0 properties
TH1F *hEpi0  = new TH1F("Epi0","Epi0",100,0.,mpi0max+2.0);
TH1F *hmpi0  = new TH1F("mpi0","mpi0",100,mpi0min-0.000001,mpi0max+0.000001);
TH1F *hppi0  = new TH1F("ppi0","ppi0",100,-0.1,2.0);
TH1F *hpxpi0 = new TH1F("pxpi0","pxpi0",100,-1.5,1.5);
TH1F *hpypi0 = new TH1F("pypi0","pypi0",100,-1.5,1.5);
TH1F *hpzpi0 = new TH1F("pzpi0","pzpi0",100,-1.5,1.5);

// pi1 (=pi-) properties
TH1F *hEpi1  = new TH1F("Epi1","Epi1",100,mpimin-0.1,mpimax+2.0);
TH1F *hmpi1  = new TH1F("mpi1","mpi1",100,mpimin-0.000001,mpimax+0.000001);
TH1F *hppi1  = new TH1F("ppi1","ppi1",100,-0.1,2.0);
TH1F *hpxpi1 = new TH1F("pxpi1","pxpi1",100,-1.5,1.5);
TH1F *hpypi1 = new TH1F("pypi1","pypi1",100,-1.5,1.5);
TH1F *hpzpi1 = new TH1F("pzpi1","pzpi1",100,-1.5,1.5);

// pi2 (=pi-) properties
TH1F *hEpi2  = new TH1F("Epi2","Epi2",100,mpimin-0.1,mpimax+2.0);
TH1F *hmpi2  = new TH1F("mpi2","mpi2",100,mpimin-0.000001,mpimax+0.000001);
TH1F *hppi2  = new TH1F("ppi2","ppi2",100,-0.1,2.0);
TH1F *hpxpi2 = new TH1F("pxpi2","pxpi2",100,-1.5,1.5);
TH1F *hpypi2 = new TH1F("pypi2","pypi2",100,-1.5,1.5);
TH1F *hpzpi2 = new TH1F("pzpi2","pzpi2",100,-1.5,1.5);

// angular distributions of pi1 (=pi-) (f2->pi-pi+)
TH1F *hcthe = new TH1F("cos(theta)", "cos(theta)", 100, -1.1, 1.1);
TH1F *hphi  = new TH1F("phi", "phi", 100, -3.5, 3.5);

// open output file for 4-vectors
TString datfn = Form("results/iso_to_pipipi_%s.dat",version.Data());
FILE *fftxt = fopen (datfn.Data(),"w");

// loop over events
Bool_t goon;
for (Int_t ii=0; ii<np; ii++) {
```

```
// ******* initial system ********
// select total momentum and energy
Eini = rnd.Uniform(Einimin,Einimax);
// p uniform in sphere
pini = sqrt(2.*rnd.Uniform(pow(ptotmin,2)/2.,pow(ptotmax,2)/2.));
// p uniform in ptot
// pini = rnd.Uniform(ptotmin,ptotmax);
mini = sqrt(pow(Eini,2)-pow(pini,2));

// select theta and phi
theta = TMath::ASin(rnd.Uniform(-1.,1.));
phi = rnd.Uniform(0.,pi2);

// commpute momentum of parent
pvini = TVector3 (
  pini * TMath::Cos(theta) * TMath::Cos(phi),
  pini * TMath::Cos(theta) * TMath::Sin(phi),
  pini * TMath::Sin(theta) );

// LorentzVector
lvini = TLorentzVector(pvini,Eini);
hEini->Fill(lvini.E(),1.);
hpini->Fill(lvini.P(),1.);
hmini->Fill(lvini.M(),1.);
hpxini->Fill(lvini.Px(),1.);
hpyini->Fill(lvini.Py(),1.);
hpzini->Fill(lvini.Pz(),1.);

// ******* f2 and pi0 *******
// let initial system decay into f2 + pi0
// select random mass for f2 within given range
// compute pf2 and ppi0 in CMS -> pf2 = -ppi0
// mf2+mpi0 < mini

goon = kTRUE;
Double_t dM2, p12;
while (goon) {
  mpi0 = rnd.Uniform(mpi0min,mpi0max<(mini-mf2min)?mpi0max:(mini-mf2min));
  mf2  = rnd.Uniform(mf2min,mf2max<(mini-mpi0)?mf2max:(mini-mpi0));
  //printf("masses %f %f %f %f",mf2,mpi0,mf2+mpi0,mini);
  goon = (mf2+mpi0>mini);

  dM2 = pow(mini,2)-pow(mf2,2)-pow(mpi0,2);
  p12 = pow(dM2/2./mini,2)-pow(mf2*mpi0/mini,2);
  goon = goon || (p12 < 0.);
  //if (goon) printf(" - bad");
  //printf("\n");
}
```

```
pf2 = sqrt(p12);

// particle energies
Ef2  = sqrt(pow(mf2,2) +p12);
Epi0 = sqrt(pow(mpi0,2)+p12);
//printf("masses: %f %f %f %f %f\n",mf2,mpi0,mf2+mpi0,mini,mini-mf2-mpi0);
//printf("Energy: %f %f %f %f %f \n",Ef2,Epi0,Ef2+Epi0,mini,mini-Ef2-Epi0);

// select direction in space
// theta and phi
theta = TMath::ASin(rnd.Uniform(-1.,1.));
phi = rnd.Uniform(0.,pi2);

// lorentz vectors of f2 and pi0
pvf2 = TVector3 (
  pf2 * TMath::Cos(theta) * TMath::Cos(phi),
  pf2 * TMath::Cos(theta) * TMath::Sin(phi),
  pf2 * TMath::Sin(theta) );
lvf2  = TLorentzVector( pvf2,Ef2);
pvpi0 = -pvf2;
lvpi0 = TLorentzVector(pvpi0,Epi0);
// printf("mf2 %f\n",lvf2.M());

// now boost the vectors with lvini
lvf2.Boost(lvini.BoostVector());
lvpi0.Boost(lvini.BoostVector());

// update histograms of f2 and pi0
hEf2->Fill(lvf2.E(),1.);
hpf2->Fill(lvf2.P(),1.);
hmf2->Fill(lvf2.M(),1.);
hpxf2->Fill(lvf2.Px(),1.);
hpyf2->Fill(lvf2.Py(),1.);
hpzf2->Fill(lvf2.Pz(),1.);
hEpi0->Fill(lvpi0.E(),1.);
hppi0->Fill(lvpi0.P(),1.);
hmpi0->Fill(lvpi0.M(),1.);
hpxpi0->Fill(lvpi0.Px(),1.);
hpypi0->Fill(lvpi0.Py(),1.);
hpzpi0->Fill(lvpi0.Pz(),1.);

// ******* pi1 (=pi-) and pi2 (=pi+) *******
// let an f2 decay into pi- + pi+
goon = kTRUE;
while (goon) {
  mpi1 = rnd.Uniform(mpimin,mpimax<(mf2-mpimin)?mpimax:(mf2-mpimin));
  mpi2 = rnd.Uniform(mpimin,mpimax<(mf2-mpi1)?mpimax:(mf2-mpi1));
  goon = (mpi1+mpi2>mf2);
```

```
    dM2 = pow(mf2,2)-pow(mpi1,2)-pow(mpi2,2);
    p12 = pow(dM2/2./mf2,2)-pow(mpi1*mpi2/mf2,2);
    goon = goon || (p12 < 0.);
  }
  ppi1 = sqrt(p12);

  // particle energies
  Epi1 = sqrt(pow(mpi1,2)+p12);
  Epi2 = sqrt(pow(mpi2,2)+p12);

  // select direction in space
  // theta and phi
  theta = TMath::ASin(rnd.Uniform(-1.,1.));
  phi = rnd.Uniform(0.,pi2);

  // lorentz vectors of pi1 (=pi-) and pi2 (=pi+)
  pvpi1 = TVector3 (
    ppi1 * TMath::Cos(theta) * TMath::Cos(phi),
    ppi1 * TMath::Cos(theta) * TMath::Sin(phi),
    ppi1 * TMath::Sin(theta) );
  lvpi1 = TLorentzVector(pvpi1,Epi1);
  pvpi2 = -pvpi1;
  lvpi2 = TLorentzVector(pvpi2,Epi2);

  // angular distributions of pi1 (=pi-) in rest frame of mother (=f2)
  hcthe->Fill(lvpi1.CosTheta(),1.);
  hphi->Fill(lvpi1.Phi(),1.);

  // now boost the vectors with lvf2
  lvpi1.Boost(lvf2.BoostVector());
  lvpi2.Boost(lvf2.BoostVector());

  // update histograms of f2 and pi0
  hEpi1->Fill(lvpi1.E(),1.);
  hppi1->Fill(lvpi1.P(),1.);
  hmpi1->Fill(lvpi1.M(),1.);
  hpxpi1->Fill(lvpi1.Px(),1.);
  hpypi1->Fill(lvpi1.Py(),1.);
  hpzpi1->Fill(lvpi1.Pz(),1.);
  hEpi2->Fill(lvpi2.E(),1.);
  hppi2->Fill(lvpi2.P(),1.);
  hmpi2->Fill(lvpi2.M(),1.);
  hpxpi2->Fill(lvpi2.Px(),1.);
  hpypi2->Fill(lvpi2.Py(),1.);
  hpzpi2->Fill(lvpi2.Pz(),1.);

              // update result file
  fprintf(fftxt,"%11.8f␣%11.8f␣%11.8f␣%11.8f\n",lvpi1.E(),
          lvpi1.Px(),lvpi1.Py(),lvpi1.Pz());
```

```
    fprintf(fftxt,"%11.8f␣%11.8f␣%11.8f␣%11.8f\n",lvpi2.E(),
            lvpi2.Px(),lvpi2.Py(),lvpi2.Pz());
                fprintf(fftxt,"%11.8f␣%11.8f␣%11.8f␣%11.8f\n",lvpi0.E(),
                lvpi0.Px(),lvpi0.Py(),lvpi0.Pz());
  }

    // clean up
    ffroot->Write();
    ffroot->Close();
    fclose(fftxt);
    return 0;
}
```

12. Appendix D

Here, we list the final parameters output of the PWA mode from PAWIAN. We have fixed all of the fit parameters which have the value zero (this is done in the configuration file), which is equivalent to excluding them from the fit.

```
L2S2_J0P-1C1Tof2(1270)_pion0Mag 60.92335515779106       0.04112341555668356
L2S2_J0P-1C1Tof2(1270)_pion0Phi 1797.895524886466       1
L2S0_f2(1270)Topion+_pion-Mag   5.49057006769636        0.003705681807846915
L2S0_f2(1270)Topion+_pion-Phi   -2633.799344224841      1
f2(1270)Mass    1.282570777986177       0.0001625203949020548   1.125   1.425
f2(1270)Width   0.1650853507175623      0.0003416948445893048   0       0.37
L1S2_J1P1C1Tof2(1270)_pion0Mag  0       0
L1S2_J1P1C1Tof2(1270)_pion0Phi  0       0
L3S2_J1P1C1Tof2(1270)_pion0Mag  0       0
L3S2_J1P1C1Tof2(1270)_pion0Phi  0       0
L0S2_J2P-1C1Tof2(1270)_pion0Mag 0       0
L0S2_J2P-1C1Tof2(1270)_pion0Phi 0       0
L2S2_J2P-1C1Tof2(1270)_pion0Mag 0       0
L2S2_J2P-1C1Tof2(1270)_pion0Phi 0       0
L4S2_J2P-1C1Tof2(1270)_pion0Mag 0       0
L4S2_J2P-1C1Tof2(1270)_pion0Phi 0       0
L1S2_J2P1C1Tof2(1270)_pion0Mag  0       0
L1S2_J2P1C1Tof2(1270)_pion0Phi  0       0
L3S2_J2P1C1Tof2(1270)_pion0Mag  0       0
L3S2_J2P1C1Tof2(1270)_pion0Phi  0       0
L1S2_J3P1C1Tof2(1270)_pion0Mag  0       0
L1S2_J3P1C1Tof2(1270)_pion0Phi  0       0
L3S2_J3P1C1Tof2(1270)_pion0Mag  0       0
L3S2_J3P1C1Tof2(1270)_pion0Phi  0       0
L5S2_J3P1C1Tof2(1270)_pion0Mag  0       0
```

```
L5S2_J3P1C1Tof2(1270)_pion0Phi  0       0
L3S2_J4P1C1Tof2(1270)_pion0Mag  0       0
L3S2_J4P1C1Tof2(1270)_pion0Phi  0       0
L5S2_J4P1C1Tof2(1270)_pion0Mag  0       0
L5S2_J4P1C1Tof2(1270)_pion0Phi  0       0
channelType1pion-pion+pion0Scaling      1       0.01    0       20
Iso1J0P-1C1     0.006557978267217934    4.603442957218373e-06   0       1
Iso1J1P1C1      0.8431073980004091      0.6573071523077467      0       1
Iso1J2P-1C1     0.4466727128856626      0.6537367957355827      0       1
Iso1J2P1C1      0.7985814896163841      0.6641060186941043      0       1
Iso1J3P1C1      0.7715197758853054      0.6669788500803686      0       1
Iso1J4P1C1      0.9999990463259867      0.5589837486969944      0       1
J0P-1C1L0S0pbarpMag     1.391080337737147       0.0009387525240548866
J0P-1C1L0S0pbarpPhi     -0.5366574235140007     1
J1P1C1L1S1pbarpMag      0.4689296751265103      1
J1P1C1L1S1pbarpPhi      0.02530966622246971     1
J2P-1C1L2S0pbarpMag     0.3382390827120106      1
J2P-1C1L2S0pbarpPhi     0.5366574218258541      1
J2P1C1L1S1pbarpMag      0.2033178475484622      1
J2P1C1L1S1pbarpPhi      1.519818035237644       1
J2P1C1L3S1pbarpMag      0.3943333896531281      1
J2P1C1L3S1pbarpPhi      -0.04656383251654829    1
J3P1C1L3S1pbarpMag      0.3779644730092272      1
J3P1C1L3S1pbarpPhi      0       1
J4P1C1L3S1pbarpMag      0.3779644730092272      1
J4P1C1L3S1pbarpPhi      0       1
```

Here, we list the final parameters output of the PWA mode from PAWIAN. All the parameters are left unfixed and are included in the fit (this is done in the configuration file).

```
L2S0_f2(1270)Topion+_pion-Mag   0.9784103308112304      0.5
L2S0_f2(1270)Topion+_pion-Phi   4573.964535398288      0.2
f2(1270)Mass    1.279573240386255       0.03    1.125   1.425
f2(1270)Width   0.162706303255204       0.037   0       0.37

L2S2_J0P-1C1Tof2(1270)_pion0Mag 4.148565601839998       0.5
L2S2_J0P-1C1Tof2(1270)_pion0Phi -1.913334221781473      0.2
L1S2_J1P1C1Tof2(1270)_pion0Mag  -2.504661237095807      0.3535533905932737
L1S2_J1P1C1Tof2(1270)_pion0Phi  3.759697021871957       0.2
L3S2_J1P1C1Tof2(1270)_pion0Mag  3.131106302711321       0.3535533905932737
L3S2_J1P1C1Tof2(1270)_pion0Phi  0.5645407540190438      0.2
L0S2_J2P-1C1Tof2(1270)_pion0Mag 0.2962424589465575      0.2886751345948129
```

```
L0S2_J2P-1C1Tof2(1270)_pion0Phi  -0.8575388862508624     0.2
L2S2_J2P-1C1Tof2(1270)_pion0Mag  0.3906717884451865      0.2886751345948129
L2S2_J2P-1C1Tof2(1270)_pion0Phi  2.281808417874992       0.2
L4S2_J2P-1C1Tof2(1270)_pion0Mag  0.5613210088790084      0.2886751345948129
L4S2_J2P-1C1Tof2(1270)_pion0Phi  -0.8572014772528469     0.2
L1S2_J2P1C1Tof2(1270)_pion0Mag   26.24005379894325       0.3535533905932737
L1S2_J2P1C1Tof2(1270)_pion0Phi   1.602717326547385       0.2
L3S2_J2P1C1Tof2(1270)_pion0Mag   12.98164415879945       0.3535533905932737
L3S2_J2P1C1Tof2(1270)_pion0Phi   -1.785577454119539      0.2
L1S2_J3P1C1Tof2(1270)_pion0Mag   0.4345358314911397      0.2886751345948129
L1S2_J3P1C1Tof2(1270)_pion0Phi   0.08314968608118349     0.2
L3S2_J3P1C1Tof2(1270)_pion0Mag   -0.08652852421596358    0.2886751345948129
L3S2_J3P1C1Tof2(1270)_pion0Phi   -0.6479243333049872     0.2
L5S2_J3P1C1Tof2(1270)_pion0Mag   0.20418666652728        0.2886751345948129
L5S2_J3P1C1Tof2(1270)_pion0Phi   -0.1071326632895575     0.2
L3S2_J4P1C1Tof2(1270)_pion0Mag   0.4783953006938912      0.3535533905932737
L3S2_J4P1C1Tof2(1270)_pion0Phi   -0.3691282296137861     0.2
L5S2_J4P1C1Tof2(1270)_pion0Mag   0.2730878479275929      0.3535533905932737
L5S2_J4P1C1Tof2(1270)_pion0Phi   0.2556303680604823      0.2

channelType1pion-pion+pion0Scaling      1       0.01    0       20
Iso1J0P-1C1     0.9999997511219094      0.5     0       1
Iso1J1P1C1      0.9999995320306601      0.5     0       1
Iso1J2P-1C1     0.999983941363576       0.5     0       1
Iso1J2P1C1      0.003731947244766276    0.5     0       1
Iso1J3P1C1      0.3685841511473129      0.5     0       1
Iso1J4P1C1      0.2420730166265156      0.5     0       1

J0P-1C1L0S0pbarpMag     0.4577516806160626      0.1889822365046136
J0P-1C1L0S0pbarpPhi     -0.5488405687827627     0.2
J1P1C1L1S1pbarpMag      0.3190611341780875      0.1889822365046136
J1P1C1L1S1pbarpPhi      -0.02554124534885023    0.2
J2P-1C1L2S0pbarpMag     0.3108144122428119      0.1889822365046136
J2P-1C1L2S0pbarpPhi     -1.497742004582022      0.2
J2P1C1L1S1pbarpMag      0.3034381986298755      0.1889822365046136
J2P1C1L1S1pbarpPhi      1.044552989112769       0.2
J2P1C1L3S1pbarpMag      -0.1624948813997236     0.1889822365046136
J2P1C1L3S1pbarpPhi      1.254505451053481       0.2
J3P1C1L3S1pbarpMag      0.3488109344309754      0.1889822365046136
J3P1C1L3S1pbarpPhi      0.02737922357583143     0.2
J4P1C1L3S1pbarpMag      0.258046899230444       0.1889822365046136
J4P1C1L3S1pbarpPhi      -0.21613590416008       0.2
```

13. References

[1] Barone, V. and Predazzi E., 2013. High-energy particle diffraction. *Springer Science & Business Media.*

[2] Donnachie, Sandy, et al. Pomeron physics and QCD. Vol. 19. Cambridge University Press, 2002. *Vol. 19. Cambridge University Press, 2002.*

[3] Chung, S.U., Brose, J., Hackmann, R., Klempt, E., Spanier, S. and Strassburger, C., 1995. Partial wave analysis in K???matrix formalism.*Annalen der Physik.* 507(5), 404-430.

[4] Peters, K., 2006. A primer on partial wave analysis. *International Journal of Modern Physics A* 21(27), 5618-5624.

[5] Chung, S.U., 2008. Spin formalisms (No. BNL-QGS-02-0900). *Brookhaven Nat. Lab..* .

[6] Richards, B. and E. Wolf., 1959. Electromagnetic diffraction in optical systems. II. Structure of the image field in an aplanatic system. *Proceedings of the Royal Society of London A: Mathematical, Physical and Engineering Sciences.* Vol. 253. No. 1274. The Royal Society, 1959.

[7] Wolf E. Electromagnetic diffraction in optical systems-I. An integral representation of the image field. *InProc. R. Soc. Lond. A 1959 Dec 15 (Vol. 253, No. 1274). The Royal Society.* 349-357.

[8] Binney, J. and Skinner, D., 2013. The physics of quantum mechanics. *Oxford University Press* .

[9] Saff, E.B. and Snider, A.D., 2003. Fundamentals of Complex Analysis with Applications to Engineering and Science,(2003). .

[10] Cohen, H., 2010. Complex analysis with applications in science and engineering.. *Springer Science & Business Media*

[11] Bateman, H. and Erdelyi, A., 1953. Higher transcendental functions (Vol. 1, No. 2). *New York: McGraw-Hill* .

[12] Levin, E., 1997. Everything about reggeons. Part I: Reggeons in" soft" interaction. *Arxiv preprint hep-ph/9710546* .

[13] Gribov, V.N., 1961. Possible asymptotic behavior of elastic scattering. *LETTERS TO THE EDITOR* 479, 1.

[14] Richman, J.D., 1984. An experimenter's guide to the helicity formalism (No. CALT-68-1148). .

[15] Schulten, K., 2000. Notes on Quantum Mechanics. *University of Illinois at UrbanaChampaign.*

[16] Amsler, C. and Bizot, J.C., 1983. Simulation of angular distributions and correlations in the decay of particles with spin. *Computer Physics Communications* 30(1), 21-30.

[17] Bressani, T., Filippi, A. and Wiedner, U. eds., 2005. Hadron Physics (Vol. 158). *IOS Press.* .

[18] Lange, D.J., 2001. The EvtGen particle decay simulation package. *Nuclear Instruments and Methods in Physics Research Section A: Accelerators, Spectrometers, Detectors and Associated Equipment*462(1-2), 152-155.

[19] Salgado, C.W. and Weygand, D.P., 2014. On the partial-wave analysis of mesonic resonances decaying to multiparticle final states produced by polarized photons. *Physics Reports* 537(1), 1-58.

[20] Patrignani, C. and Particle Data Group, 2016. Review of particle physics. *Chinese physics C*40(10), 100001.

[21] Peskin, M.E., 1995. An introduction to quantum field theory. *Westview press*

[22] Bevan, A. and Wilson, F., 2010. AFit User Guide. *Technical report, Dec 2010. List of Figures.*.

[23] Outa, H., 2005. Hadron Physics, Proceedings of the International School of Physics Enrico Fermi, Course CLVIII, Varenna, Italy. .

[24] Brun, R. and Rademakers, F., 1997. ROOT???an object oriented data analysis framework. *Nuclear Instruments and Methods in Physics Research Section A: Accelerators, Spectrometers, Detectors and Associated Equipment* 389(1-2),81-86.

[25] Morrison, M.A. and Parker, G.A., 1987. A guide to rotations in quantum mechanics. *Australian journal of physics* 40(4), 465-498.

List of Figures